YALE
PEABODY
MUSEUM

JOURNAL OF MARINE RESEARCH

The *Journal of Marine Research,* one of the oldest journals in American marine science, published important peer-reviewed original research on a broad array of topics in physical, biological, and chemical oceanography vital to the academic oceanographic community in the long and rich tradition of the Sears Foundation for Marine Research at Yale University.

An archive of all issues from 1937 to 2021 (Volume 1–79) are available through EliScholar, a digital platform for scholarly publishing provided by Yale University Library at https://elischolar.library.yale.edu/.

Requests for permission to clear rights for use of this content should be directed to the authors, their estates, or other representatives. The *Journal of Marine Research* has no contact information beyond the affiliations listed in the published articles. We ask that you provide attribution to the *Journal of Marine Research.*

Yale University provides access to these materials for educational and research purposes only. Copyright or other proprietary rights to content contained in this document may be held by individuals or entities other than, or in addition to, Yale University. You are solely responsible for determining the ownership of the copyright, and for obtaining permission for your intended use. Yale University makes no warranty that your distribution, reproduction, or other use of these materials will not infringe the rights of third parties.

Sensitivity of plankton biomass and productivity to variations in physical forcing and biological parameters in Chesapeake Bay

by Ming Li[1,2], Liejun Zhong[1,3] and Lawrence W. Harding, Jr.[1]

ABSTRACT

A coupled three-dimensional hydrodynamic-biogeochemical model is used to simulate plankton dynamics in Chesapeake Bay and examine its sensitivity to variations in biological parameters and physical forcing. The coupled biophysical model captures observed seasonal cycle and regional distributions of plankton in Chesapeake Bay and predicts the "phase lag" between the spring chlorophyll maximum and the summer primary productivity maximum. This lag traces to the delivery of dissolved inorganic nutrients in the winter-spring freshet from the Susquehanna River that fuels the spring bloom, whereas regenerated nutrients support high primary productivity in summer. The model shows that episodic wind events commonly associated with frontal passages in summer inject nutrients into the euphotic layer, leading to short periods of elevated primary productivity. Quantitative comparisons between the predicted and observed annual time series of euphotic-layer chlorophyll and primary productivity show that the model possesses reasonable skill. Sensitivity analyses of model simulations for different biological parameter values and alternative formulations of biogeochemical processes suggest that model predictions are robust. To understand the impacts of climate variability and change on Chesapeake Bay, we examine how the plankton system responds to variations in river runoff, wind forcing, temperature and light level. Annual mean chlorophyll (AMC) and annual integrated production (AIP) increase by about 70% for a doubling of river runoff, but only reduce by 30% and 13% for 50% reduction of river runoff, suggesting a nonlinear response of plankton system to changes in river runoff and nutrient loading. Doubling of wind stress results in a small increase in AMC but 28% increase in AIP. For 2°C warming AMC increases from 25.4 to 30 mg m^{-2} and AIP increases from 180 to 246 g C m^{-2} yr^{-1}.

1. Introduction

The Mid-Atlantic coast of the United States is indented by a number of large and productive estuaries, connecting varied landscapes to receiving waters of the coastal ocean. These estuaries display strong seasonal to interannual variability of key ecosystem properties and processes, reflecting both anthropogenic and climatic influences. Over the past 50 years, nutrient enrichment has led to increased phytoplankton biomass as chlorophyll *a* (*chl-a* hereafter) in large estuaries such as Chesapeake Bay (Harding and Perry,

1. Horn Point Laboratory, University of Maryland Center for Environmental Science, P. O. Box 775, Cambridge, Maryland, 21613, U.S.A.
2. Corresponding author. *email: mingli@umces.edu*
3. Present address: CSIRO Marine and Atmospheric Research, Floreat, WA 6014, Australia.

1997), and tributaries such as the Neuse River draining into the Albemarle-Pamlico Sound (Paerl *et al.,* 2006). Recent analyses of shipboard and remotely sensed *chl-a* for Chesapeake Bay, however, show that seasonal to interannual variability of phytoplankton biomass in the last two decades is strongly linked to climate variability (Harding *et al.,* 2002; Adolf *et al.,* 2006; Miller and Harding, 2007).

Chesapeake Bay is a partially mixed estuary. The Susquehanna River at the northern extreme of the Bay provides approximately 60% of the total freshwater input but over 80% of allochthonous nutrients (Malone *et al.,* 1988). A spring phytoplankton bloom develops from April to mid-May, representing the annual peak of phytoplankton biomass (Malone, 1992). By mid- to late-May, strong density stratification develops, isolating the surface mixing layer from the bottom layer (Carter and Pritchard, 1988). Organic material derived from sinking phytoplankton provides the substrate to support a robust microbial community whose metabolic activities regenerate nutrients to support summer phytoplankton production (Kemp *et al.,* 1990; Kemp and Boynton, 1992). During summer, integrated, water-column *chl-a* is lower than in spring, whereas primary productivity (PP hereafter) reaches an annual maximum (Malone *et al.,* 1988). This annual cycle consisting of displaced peaks of spring biomass and summer PP is a notable characteristic of Chesapeake Bay (Malone, 1992).

In addition to the strong seasonal cycle, phytoplankton in Chesapeake Bay exhibits large interannual variability in response to changes in freshwater inflow and nutrient loading. Malone *et al.* (1988) showed that flow from the Susquehanna River accounted for a significant amount of the variance of phytoplankton biomass in 1985–86. A lengthy time-series from aircraft remote sensing (1989–present) has since confirmed this view, linking interannual variability of *chl-a* in the spring bloom to regional climate forcing (Miller *et al.,* 2006a; Miller and Harding, 2007). Furthermore, Harding *et al.* (2002) found that AIP by phytoplankton is strongly correlated to freshwater flow and nutrient loading in winter-spring. Miller *et al.* (2010) showed that climate variability forces two- to three-fold interannual variability of AIP, with lower production in drought years and higher production in flood years.

These observational studies suggest that climatic processes exert important controls on plankton dynamics in the Bay (e.g. Boicourt, 1992), but mechanisms linking climate variability and PP are not well understood. Several fundamental questions concerning phytoplankton dynamics in Chesapeake Bay remain unanswered: (1) How does winter-spring runoff control the timing, size, and regional distribution of spring phytoplankton bloom? (2) How do summer winds influence the re-supply of nutrients to the surface mixing layer, affecting PP in the Bay? (3) How does climatic variability underlying drought-flood cycles regulate phytoplankton dynamics in the Bay?

To address these questions, we have coupled a biogeochemical model with a realistic three-dimensional (3D) hydrodynamic model of Chesapeake Bay that captures responses of the physical system to climatic and meteorological forcing. The hydrodynamic model is based on the state-of-art Regional Ocean Modeling System (ROMS) and has been

validated using time-series of sea level, temperature, salinity and currents at a number of monitoring stations, and data from 3D synoptic hydrographic surveys (Li *et al.,* 2005, 2006, 2007; Zhong and Li, 2006; Zhong *et al.,* 2008; Li and Zhong, 2009). The model shows considerable capability to reproduce estuarine dynamics at seasonal and interannual time-scales (Li *et al.,* 2005; North *et al.* 2008; Hilton *et al.,* 2008).

The biogeochemical model is a simple five-component model that we have adapted to simulate plankton dynamics in Chesapeake Bay. Similar modeling approaches have been taken in other investigations. For example, Moisan *et al.* (1996) coupled a nine-component food web model with a 3D model of the California coastal transition zone to investigate how physical processes affect spatial and temporal distributions of nutrients and plankton. Fennel (1999) coupled a 3D circulation model with a four-compartment plankton model to investigate regional and interannual variability of biological variables in the Western Baltic Sea. Chen *et al.* (2001) and Franks and Chen (2001) coupled a nutrient-phytoplankton-zooplankton (NPZ) model with the 3D Princeton Ocean Model to investigate how tidal mixing affects plankton productivity in Georges Bank and Nantucket Shoals. Fennel *et al.* (2006) developed a coupled hydrodynamic-biogeochemical model to study nitrogen cycling and export in the Mid-Atlantic Bight. Although the biogeochemical models used in these studies are relatively simple, they have provided important insights into the physical and biogeochemical processes that control plankton productivity and nutrient cycling in the coastal ocean.

More complex biogeochemical models, such as the water-quality model commissioned by the EPA Chesapeake Bay Program (CBP) and developed by the U.S. Army Corp of Engineers, have been used to assist policy makers and resource managers to design nutrient-reduction strategies for Chesapeake Bay (Cerco and Cole, 1993; Cerco, 1995). This water quality model has 22 compartments and over 100 parameters (e.g., Cerco and Cole, 1993; Cerco, 1995), including dissolved oxygen, multiple forms of algae, carbon, nitrogen, phosphorus and silica. Given its complexity, this model cannot be easily applied to explore basic questions regarding the climatic control of plankton dynamics in Chesapeake Bay. Recently, Xu and Hood (2006) coupled an eight-compartment biogeochemical model to the CBP CH3D hydrodynamic model (Johnson *et al.,* 1993) and retrieved certain water-quality parameters along the central axis of the Bay. However, that application of the model had some limitations including the over-prediction of phytoplankton biomass in shoal regions and the over-prediction of oxygen concentrations in deep channels.

In this paper we use the newly-developed hydrodynamic-biogeochemical model to investigate the annual cycle and regional distributions of plankton biomass and productivity in Chesapeake Bay. Our goal is to gain insights into key physical and biological processes that control the plankton dynamics in the Bay. The paper is organized as follows. Section 2 describes the model configuration while Section 3 presents model simulation results and comparisons with observations. Section 4 examines the sensitivity of key plankton metrics to changes in physical/climatic forcing and biological rate parameters. These numerical experiments illustrate how the plankton system might respond to
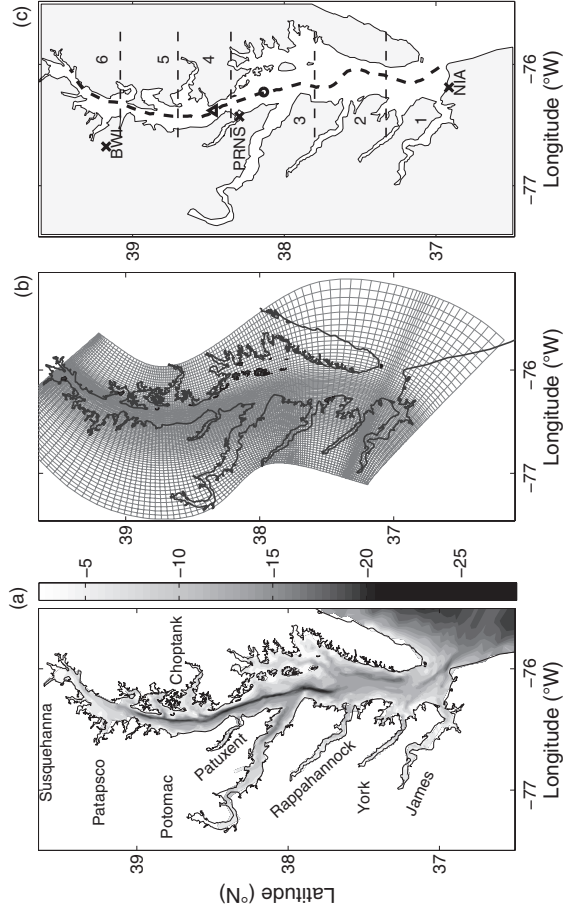
Figure 1. (a) Bathymetry of Chesapeake Bay and the adjacent coastal area. Major tributaries are shown. Depths are in meters; (b) horizontal curvilinear coordinate system designed for resolving the complex coastlines and the deep channel in the Bay; (c) Locations of the longitudinal transect (thick dashed line) and latitudinal boundaries (thin dashed lines) of regions (1–6) used in the model analysis and previous observational studies. The triangle and circle represent the CBOS (Chesapeake Bay Observing System) mid-Bay station and CB5.2 station, respectively. Crosses represent airport stations where wind measurements were made.

climatically-driven variations in river runoff, wind forcing and temperature. Concluding remarks are given in Section 5.

2. Model description

a. Hydrodynamic model

ROMS is a regional ocean model. It is well suited for coupling with biogeochemical models as it incorporates advanced numerical schemes for advecting tracers (Shchepetkin and McWilliams, 2005), and sophisticated turbulence closure schemes to parameterize turbulent mixing (Warner *et al.,* 2005b). We have configured the ROMS hydrodynamic model for Chesapeake Bay, as described by Li *et al.* (2005). Here we summarize main elements of the model relevant to this paper. An orthogonal curvilinear coordinate system is designed to follow the general orientation of the deep channel and the coastlines of the main stem Bay (Fig. 1a, b). The model has 1 km resolution in the horizontal direction and 20 vertical layers. The stretching parameters for the vertical grid are $\theta_S = 2$ and $\theta_B = 0.8$, as defined in the S-coordinate system (Song and Haidvogel, 1994). Vertical eddy viscosity and diffusivity are computed using the *k-kl* turbulence mixing scheme incorporated into ROMS (Warner *et al.,* 2005b).

The hydrodynamic model is forced by open-ocean tides, freshwater inflows at river heads, and wind and heat exchange across the water surface. At the open ocean boundary, sea level is updated using data from stations at Wachapreague, Virginia and Duck, North Carolina obtained from the National Ocean Service. Salinity and temperature fields at the offshore open boundary are prescribed using monthly Levitus climatology combined with field data from Duck, North Carolina acquired by the Field Research Facility of the U.S. Army Corps of Engineers. At the upstream boundary in eight major tributaries, daily freshwater inflow with zero salinity and time-varying temperature is prescribed. We select the year of 1997 for model simulations as annual discharge from the Susquehanna River into the Bay was close to the historical average. As shown in Figure 2a, the discharge from the Susquehanna River shows a typical seasonal cycle: high discharge during the winter-spring period, low discharge during the summer and early fall, and high discharge again in late fall.

CBP collects monitoring data at 88 stations throughout the Bay. We construct a sea surface temperature (SST) field using temperature measurements from these monitoring stations. Modeled SST is relaxed toward this temperature field with a fast time scale of 6 h. Since no heat flux measurements are available over Chesapeake Bay, the relaxation boundary condition provides a simple but effective way to obtain SST forcing for the model, as done in other ocean circulation models (e.g. Lima and Doney, 2004). Figure 3a shows the annual cycle of SST at the mid-Bay station CB5.2 (see Fig. 1c for its location). It is clear that the model captures the observed seasonal change of SST really well.

To apply the wind forcing over the surface of Chesapeake Bay, hourly wind stress in the mid- to lower Bay is linearly interpolated from data collected at the Norfolk International Airport (NIA), Patuxent River Naval Station (PRNS), and Baltimore-Washington International Airport (BWI). North of BWI, the wind stress is assumed to be identical to that at
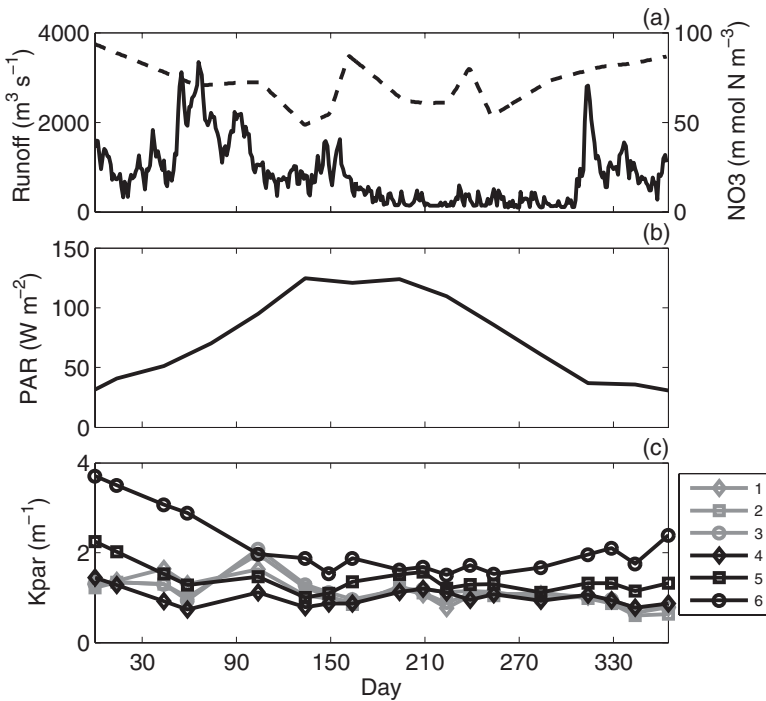
Figure 2. (a) Time series of river runoff (solid line) and NO_3 concentration (dashed line) at Susquehanna River; (b) Time series of surface value of Photosynthetically Available Radiation (PAR); (c) regionally-averaged light attenuation coefficients obtained from Secchi disk readings.

BWI. Winds over Chesapeake Bay are episodic with dominant periods of 2–7 days (Wang, 1979a; b). Northwesterly winds dominate in winter months whereas southerly winds of several days duration are more frequent in the summer. An example of wind-stress time series is shown in Figure 8a.
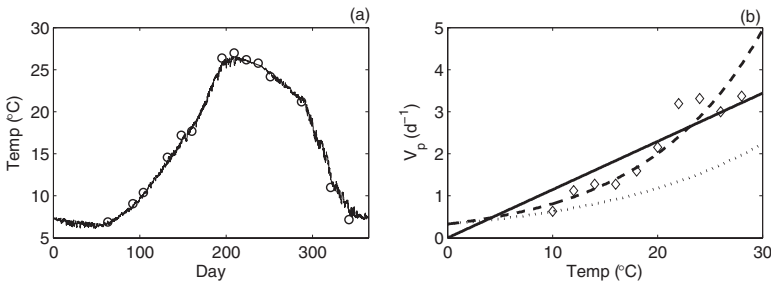

Figure 3. (a) Model-derived (black line) and observed (open circles) sea surface temperature at CB5.2 station; (b) Maximum phytoplankton growth rate as a function of temperature: the diamonds represent data collected in Chesapeake Bay, the solid line is the linear fit, the dashed line an exponential fit and dotted line the Eppley's curve.

b. Biogeochemical model

A recent review of biogeochemical and water quality models indicates that those of intermediate complexity tend to have the highest predictive skill (Arhonditsis and Brett, 2004). This analysis led to our selection of a five-compartment (nitrate or NO_3, ammonium or NH_4, phytoplankton, zooplankton, and detritus) biogeochemical model based on Fasham *et al.* (1990). To apply this model to a shallow-water estuary such as Chesapeake Bay, we have considered additional biogeochemical processes and made several model modifications.

The equations for the five-compartment biogeochemical model are given by

$$\frac{d[NO_3]}{dt} = -t_{PP\max} \cdot Q_{NP} \cdot [Phyto], \tag{1}$$

$$\frac{d[NH_4]}{dt} = -t_{PP\max} \cdot Q_{RP} \cdot [Phyto] + (t_{Zbmet} + Q_{excr}) \cdot [Zoo] + t_{Dremin} \cdot [Det], \tag{2}$$

$$\frac{d[Det]}{dt} = Q_{graze} \cdot (1 - AE_N) \cdot [Zoo] + t_{Pmort} \cdot [Phyto]$$
$$+ t_{Zmort} \cdot [Zoo]^2 - t_{Dremin}[Det] - L_{vd}\frac{\partial[Det]}{\partial z}, \tag{3}$$

$$\frac{d[Phyto]}{dt} = t_{PP\max} \cdot (Q_{NP} + Q_{RP}) \cdot [Phyto]$$
$$- t_{Pmort} \cdot [Phyto] - Q_{graze} \cdot [Zoo] - L_{vp}\frac{\partial[Phyto]}{\partial z}, \tag{4}$$

$$\frac{d[Zoo]}{dt} = Q_{graze} \cdot AE_N \cdot [Zoo] - (t_{Zbmet} + Q_{excr}) \cdot [Zoo] - t_{Zmort} \cdot [Zoo]^2. \tag{5}$$

where the parameters include phytoplankton mortality rate t_{Pmort} and sinking speed L_{vp}, zooplankton grazing rate t_{Zgraz}, grazing efficiency AE_N, metabolism rate t_{Zbmet}, excretion rate Q_{exert} and mortality rate t_{Zmort}, detritus sinking speed L_{vd} and remineralization rate t_{Dremin}. The functions used in (1)–(5) are:

$$Q_{NP} = \frac{[NO_3]}{K_{NO_3} + [NO_3]} \cdot \frac{1}{1 + [NH_4]/K_{NH4}}, \tag{6}$$

$$Q_{RP} = \frac{[NH_4]}{K_{NH4} + [NH_4]}, \tag{7}$$

$$Q_{graze} = t_{Zgraze} \cdot \frac{[Phyto]^2}{K_p^2 + [Phyto]^2}, \tag{8}$$

$$t_{PP\text{max}} = f(PAR) = \frac{V_p \cdot \alpha \cdot PAR}{\sqrt{V_P^2 + \alpha^2 PAR^2}}. \tag{9}$$

The growth rate of phytoplankton depends on: temperature (Temp) through the maximum growth rate V_P; photosynthetically available radiation (PAR) and nutrient concentrations (NO_3, NH_4). The function f(PAR) represents the photosynthesis-light (P-I) relationship (Evans and Parslow, 1985), where α is the initial slope and V_P is the maximum growth rate. In Chesapeake Bay, α increases from $\sim$0.048 in spring to $\sim$0.065 [molC gChl^{-1}(Wm^{-2})$^{-1}$d^{-1}] in summer (Harding *et al.,* 2002).

In the biogeochemical model we lump all phytoplankton groups into one compartment. The flora of Chesapeake Bay is dominated by diatoms on an annual scale. Other taxonomic groups that are significantly represented include flagellates and cyanobacteria, but even in summer diatoms comprise most of *chl-a.* Responses of the flora to freshwater inputs and nutrient loading are strongly manifested in the diatom signature and covary with *chl-a,* as documented by Adolf *et al.* (2006). Thus, the plankton responses to physical/climate forcing can be well quantified with a biogeochemical model that captures variability of *chl-a.*

The empirical function of V_P by Eppley (1972) was originally developed for open ocean applications and cannot be directly applied to Chesapeake Bay. Figure 3b shows how the observed maximum phytoplankton growth rate (binned-averaged over 2°C increments) varies with water temperature in the Bay using *chl-a* and PP data from Harding *et al.* (2002) and assuming C:*chl-a* = 40. We fit the data with a linear function:

$$V_p = 0.11465 \, Temp \tag{10}$$

with the regression correlation coefficient $r^2 = 0.967$. Alternatively, one can fit an exponential function:

$$V_p = 0.32949 \, e^{0.090246 \, Temp} \tag{11}$$

with $r^2 = 0.848$. For comparison, we also fit Eppley's curve given by:

$$V_p = 0.32949 \times 1.066^{Temp}. \tag{12}$$

These empirical formulae will be used in the biogeochemical model instead of Eppley's original equation. As shown in Figure 3, the temperature increases from 5°C in winter to 25°C in summer, which can lead to a five-fold increase in the phytoplankton growth rate.

Water clarity is affected by chromophoric dissolved organic material (CDOM), suspended particulate material (SPM), and pigments (including *chl-a*) in the water column. In Chesapeake Bay, sediment loading is a major factor determining water clarity. We prescribe surface *PAR* (Photosynthetically Available Radiation) values using Fisher *et al.* (2003) measurements and a light-attenuation coefficient using Harding *et al.* (2002) optical measurements. Two time-series of surface PAR are obtained from observations at the Smithsonian Environmental Research Center (SERC) and Horn Point Laboratory (HPL) on the western and eastern shores of the mesohaline Bay, respectively. The annual cycle of

PAR shows a nearly sinusoidal variation over the year (Fig. 2b). We draw on an extensive data set on light attenuation coefficient, K_{PAR}, estimated from Secchi disk readings (Harding, unpublished) and calibrated against vertical profiles obtained with a submersible quantum meter (Li-Cor model 192S). K_{PAR} is linearly interpolated from biweekly to monthly sampling cruises and aggregated to form averages for six regions of the Bay defined by Harding and Perry (1997) (Fig. 1c). As the predominant source of CDOM and SPM is the Susquehanna River at the northern end of the Bay, K_{PAR} attains much higher values in the upper Bay and decreases toward the lower Bay (Fig. 2c). This north-south gradient is most pronounced during the spring freshet but is also significant in fall. Optical measurements from CBP monitoring cruises produce reasonable estimates of K_{PAR} for most regions of the Bay. However, in the upper Bay regions (5 and 6) close to the estuary's head, monitoring data are collected along the center shipping channel where water is significantly less turbid than other parts of the upper Bay. These stations give low values of K_{PAR}, but we cannot quantify this bias due to the lack of measurements on the shoal regions. As a preliminary step, we apply an empirical amplification factor (double K_{PAR} in regions 5 and 6) to correct for this underestimate of K_{PAR}. Without this factor, the model overestimates *chl a* and PP in the upper Bay, as shown in Figures 13 g and h (to be discussed in Section 4a). In their modeling study, Xu and Hood (2006) also found that their model overestimated PP in the upper Bay. They subsequently applied an empirical factor to reduce the maximum phytoplankton growth rate from 3.22 to 0.96 d^{-1} in regions where salinity is lower than 3 psu. They suggested consumption by benthic bivalves, senescence in the transition zone from fresh to saline water, and differences in species composition as possible causes for the declines in phytoplankton growth rate in the upper Bay. We think that the under-sampling of K_{PAR} is more likely the cause for the model overestimates of *chl a* and PP there. Finally, we note that the model predictions for the middle and lower Bay are relatively unaffected by those for the upper Bay (see Fig. 13).

Based on the observations by Malone *et al.* (1996), we consider nitrogen to be the key nutrient limiting phytoplankton growth in the biogeochemical model. However, it has been shown that phytoplankton growth may be limited by phosphorus (P) in freshwater and by nitrogen (N) availability in saline waters of the Bay. Fisher *et al.* (1992; 1999) found that P limits phytoplankton growth in the upper Bay during high runoff. Because N and P cycles in estuarine systems are decoupled in many respects, proper representation of the P cycle in the Chesapeake Bay requires fairly explicit modelling. In order to avoid this level of complexity, and considering that P-limitation is significant only during spring and that there are only small differences in dissolved inorganic phosphorus (DIP) over whole Bay (Fisher *et al.,* 1992), we use the approach of Xu and Hood (2006), assign a uniform value for DIP over the whole Bay, and specify how this value varies seasonally relative to a fixed half-saturation constant for P uptake in the model.

Observations in the Bay suggest that PP in summer is related to nutrient inputs during winter-spring via organic deposition coupled to temperature-dependent benthic decompo-

sition and nutrient regeneration (e.g. Kemp *et al.,* 1990; Kemp and Boynton, 1992). Dead plankton derived from the spring bloom sinks into the bottom layer and is remineralized into ammonium by microbial activity that is maximal during the warm summer. We devise a simple parameterization for this nutrient regeneration process by allowing "dead" plankton (detritus) to sink to bottom waters and apply a temperature-dependent remineralization rate. Lomas *et al.* (2002) examined how microbial rate processes responded to temperature and found them to lie in a constrained range of Q_{10} (the factor increase in a rate process for a 10°C increase of temperature). Using $Q_{10} = 2.5$, we construct an empirical function for the remineralization rate t_{Dremin}:

$$t_{Dremin} = \begin{array}{ll} 0.05 Q_{10}^{0.1(Temp-3)} & \text{for Temp} \geq 3°\text{C} \\ 0.05 & \text{for Temp} < 3°\text{C} \end{array} \tag{13}$$

Lomas *et al.* (2002) also noted that the upper bounds on all of the microbial rate processes could be described well by a linear function of temperature. From their Figure 8, we construct another empirical function given by:

$$t_{Dremin} = \begin{array}{ll} 0.05 + 0.45(Temp - 3)/25 & \text{for 28°C} \geq \text{Temp} \geq 3°\text{C} \\ 0.05 & \text{for Temp} < 3°\text{C} \\ 0.5 & \text{for Temp} > 28°\text{C} \end{array} \tag{14}$$

In the sensitivity analysis presented in Section 4, we find that model results are insensitive to the detailed functional form, provided that t_{Dremin} is temperature-dependent. To account for the effects of sediment biogeochemistry on the overlying water column, we specify a denitrification rate as a linear function of ambient NO_3 in bottom water, according to results from laboratory experiments (Kana *et al.,* 1998). Hence, in the NO_3 equation for the bottom-most layer, we add a "sink term" proportional to the ambient NO_3 concentration. Fennel *et al.* (2006) developed a more sophisticated benthic model by setting the remineralization rate for deposited organic matter in the upper part of the sediment as a bottom boundary condition. Such a model could be modified to include temperature-dependent effects, but we do not pursue this option here.

As shown in Eq. 8, zooplankton grazing on phytoplankton is represented by a Holling-type curve with K_P as the half-saturation coefficient. Zooplankton populations in the Bay include both slow-growing meso-zooplankton and fast-growing micro-zooplankton (c.f. Johnson *et al.,* 2003; White and Roman, 1992). Using one zooplankton compartment to represent both size-classes is a modeling simplification we adopted. As a first step beyond prescribing constant grazing pressure, we use a seasonally varying grazing rate that is intended to capture higher grazing rates by micro-zooplankton during summer; t_{Zgraze} is 0.15 in summer (between day 180 and 240), 0.1 during winter and fall (before 120 day and after 300 day), and linear variation during the two transition periods. A quadratic mortality

rate is used to parameterize density-dependent effects in the predation of zooplankton (Steel and Henderson, 1992).

To run the coupled model, we need to prescribe the boundary and initial conditions for the biogeochemical model. The boundary conditions for the biogeochemical model include the prescription of nutrient concentrations and plankton biomass at the river heads and open boundary as well as the PAR value at the Bay's surface. Time series for NO_3 in the Susquehanna River show concentrations ranging from 50 to 90 m Mol N m^{-3} for 1997 (Fig. 2a). High runoff in spring delivers a NO_3 pulse to the main stem Bay that supports the spring bloom. Other tributaries contribute to nutrient loading, but in this paper we focus on inputs from the Susquehanna because these represent 80% of total nitrogen loading to the main stem, and it is not straightforward to quantify nutrient loading from other sources. Boynton *et al.* (1995) analyzed the total nitrogen (TN) budget for Chesapeake Bay and found that TN is exported from the Bay. Cerco and Cole (1993) and Cerco (1995) also noted that most of the nutrient loads into Chesapeake Bay come from the tributaries. Hence the nutrient input from the shelf is expected to be small. Due to the lack of continuous nutrient measurements near the model's open boundary, we set NO_3 and NH_4 concentrations at the low value of 1 m Mol N m^{-3} there.

For the initial condition, we prescribe sea level, velocity, temperature, salinity, nutrients and plankton fields at the beginning of 1997. The initial velocity field is taken to be zero, and the water surface is set at the mean sea level. To set initial conditions for salinity and temperature, we run the hydrodynamic model for 1996 and use the model-predictions at year end. It should be mentioned that the outputs of the hydrodynamic model have been validated against observations for 1996 (Li *et al.,* 2005). The initial NO_3 and phytoplankton fields are interpolated from EPA CBP survey data, whereas the initial fields for other biogeochemical variables are set at low concentrations due to a lack of sufficient observations for winter.

3. Seasonal cycle and regional distributions

In this section we show the results from the control run (Run C) and compare model results with observations. Table 1 gives the definitions of the model parameters, their units and the values used in Run C.

a. NO$_3$ delivery by freshwater plume and development of spring bloom

First we examine the model-predicted circulation pattern and salinity distribution in Chesapeake Bay. Figure 4a shows tidally averaged residual surface currents in March 1997. Freshwater originating from the Susquehanna River spreads south as a plume with currents that reach 0.2 m s^{-1}. The plume covers the whole width in the upper Bay, but is confined to the western shore in the mid Bay due to the effect of Coriolis force. It expands

Table 1. Definition of biogeochemical parameters and parameter values used in the control run (Run C).

Symbol	Parameter	Value	Unit
V_p	Phytoplankton maximum growth rate	Temperature dependent formulas (Eq. 10)	d^{-1}
α	Initial slope of the P-I curve	0.065	molC gChl^{-1} (Wm^{-2})$^{-1}$d^{-1}
K_{NO3}	Half-saturation concentration for uptake of NO_3	1	m mol N m^{-3}
K_{NH4}	Half-saturation concentration for uptake of NH_4	1	m mol N m^{-3}
t_{Pmort}	Phytoplankton mortality rate	0.01	d^{-1}
t_{Zgraze}	Maximum grazing rate	Seasonally varying	d^{-1}
AE_N	Grazing efficiency	0.7	dimensionless
K_p	Half-saturation concentration for zooplankton grazing	1	m mol N m^{-3}
t_{Zmot}	Zooplankton mortality rate	0.006	(m mol N m^{-3})$^{-1}$ d^{-1}
t_{Zbmet}	Excretion rate due to basal metabolism	0.007	d^{-1}
Q_{excr}	maximum rate of assimilation related excretion	0.007	d^{-1}
L_{vp}	Phytoplankton sinking rate	0.1	m d^{-1}
L_{vd}	Detritus sinking rate	1	m d^{-1}
t_{Dremin}	Detritus remineralization rate	Temperature-dependent formulas (Eq. 13)	d^{-1}

laterally in the lower Bay before exiting as a buoyancy-driven boundary current along the coast. In a vertical section aligned along the north-south axis of the Bay, residual velocity shows a two-layer flow with the surface layer moving seaward and the bottom layer moving landward (Fig. 4b). The depth of no-motion separating the two layers occurs at 5–8 m, similar to the euphotic-layer depth. Strong water-column stratification is established following high river discharge in earlier months (Fig. 4c).

The estuarine circulation provides an effective mechanism for transporting terrestrially derived nutrients seaward in Chesapeake Bay. Figure 5 shows the model-predicted temporal evolution of surface NO_3 and *chl-a* from February to May 1997. At day 30, a plume of high NO_3 spread down the Bay by the seaward-moving surface current (Fig. 5a), and by day 75 NO_3 was depleted in the lower Bay and a significant part of the mid-Bay (Fig. 5b). At day 125, high NO_3 was restricted to the upper Bay as phytoplankton uptake had consumed NO_3 along the main stem axis (Fig. 5c). Nutrient delivery by the freshwater plume coincided with seasonal increases of light and temperature (see Figs. 2b and 3a), creating optimal conditions for phytoplankton growth during the spring. The "NO_3 drawdown" was associated with an intense spring bloom that covered the region between
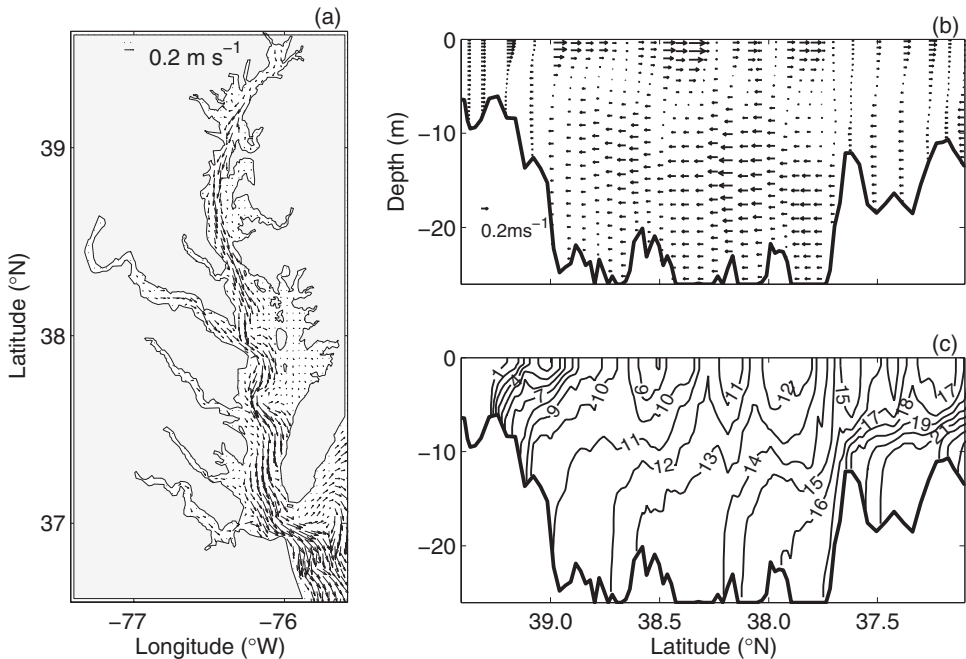
Figure 4. (a) Horizontal distribution of tidally averaged velocity at the surface of Chesapeake Bay; (b) vertical distribution of tidally averaged velocity along the center channel; (c) along-channel distribution of tidally averaged salinity in Chesapeake Bay, all for day 75 (midMarch).

37.5° and 38.6° N. latitude (Figs. 5d–f). The spring bloom commonly occurs in this area because nutrients become limiting toward the mouth of the Bay, whereas light limits phytoplankton growth in turbid waters near the head of Bay. By day 125, plankton biomass had declined significantly.

Snapshots of NO_3, NH_4, phytoplankton and zooplankton distributions in an along-channel vertical section provide further insights to spring bloom dynamics. In Figure 6, we present model outputs for mid-March (day 75) when the bloom reached its peak, as confirmed by observations presented in Figure 9. In much of the uppermost Bay, water depths are <5 m and flows were directed seaward at all depths such that NO_3 was essentially exported from the Susquehanna River. Further south, NO_3 was carried seaward by the freshwater plume, but also leaked into the lower layer due to turbulent mixing. Because of the estuarine return flow, nutrients were mostly retained inside the Bay rather than being exported to the shelf (see Fig. 4b). In contrast to high NO_3, NH_4 was low throughout the Bay in mid-March. This is consistent with the accepted paradigm that allochthonous nutrients from the watershed dominated by NO_3 largely fuel the spring bloom. Vertical distributions of *chl-a* show higher concentration of phytoplankton to a depth of ~10 m, and also reveal a *chl-a* signal in bottom waters traceable to sinking (Fig. 6c). As the growth rate of zooplankton is much lower than that of phytoplankton in
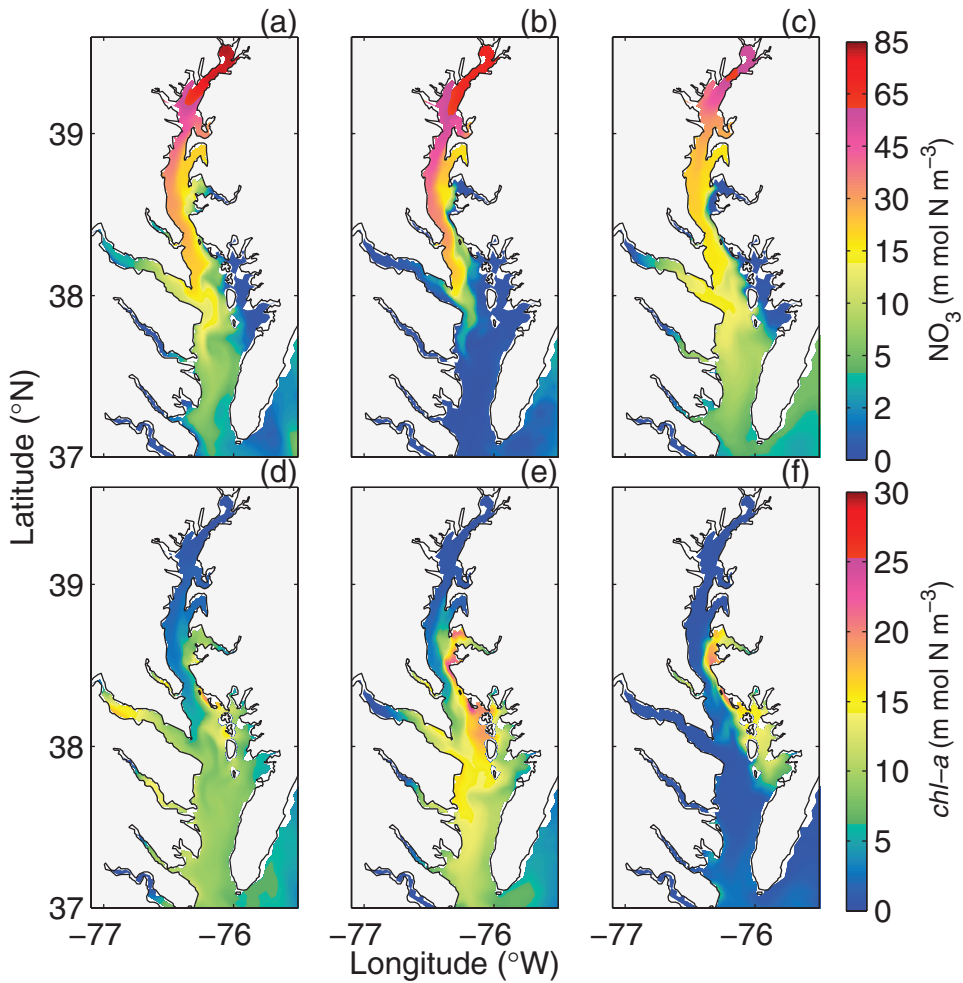
Figure 5. Surface distributions of NO_3 and *chl-a* at day 30 (a/d), 75 (b/e) and 125 (c/f).

late winter to early spring, zooplankton was at relatively low abundances in March, a pattern captured by the model (Fig. 6d).

b. *Nutrient recycling and summer productivity*

Figure 7 shows the model-predicted along-channel distributions of NO_3, NH_4, phytoplankton and zooplankton during the summer (day 210). Comparing Figures 7a and 7b shows that NH_4 greatly exceeded NO_3, consistent with observations that summer PP is largely supported by regenerated nutrients. Phytoplankton reached high concentrations only in the upper Bay and moderate concentrations in the surface layer of mid-Bay
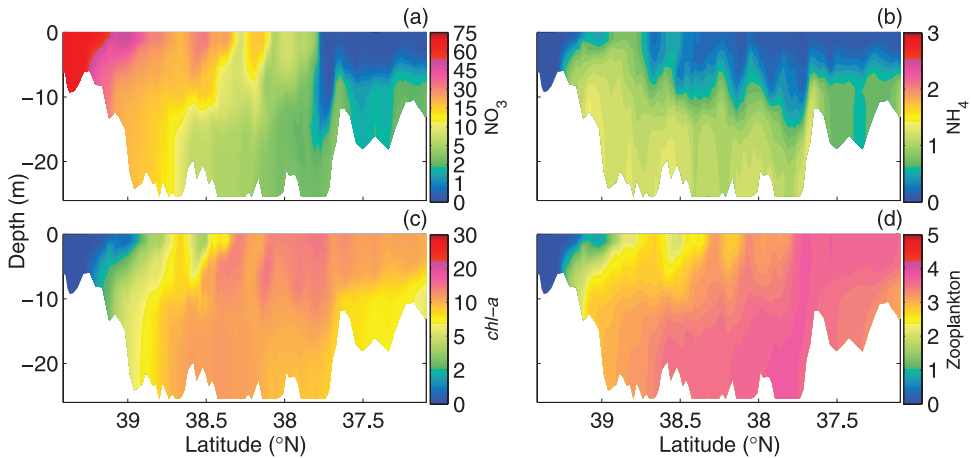
Figure 6. Distributions of (a) NO_3, (b) NH_4, (c) phytoplankton (*chl-a*), (d) zooplankton in an along-channel section at day 75 (mid March), all in units of m Mol N m^{-3}.

(Fig. 7c), and zooplankton grazed on phytoplankton and grew into sizeable populations in summer (Fig. 7d).

Kemp and Boynton (1992) suggested that dead plankton sinks and is remineralized to yield regenerated nutrients that support high PP in summer. However, the mechanism for reintroduction of regenerated nutrients into the euphotic layer under the strongly stratified conditions that persist in the summer has not been satisfactorily explained. With the coupled biophysical model, we explored possible physical mechanisms responsible for the nutrient supply. Figure 8 shows the model-predicted time-depth distribution of eddy
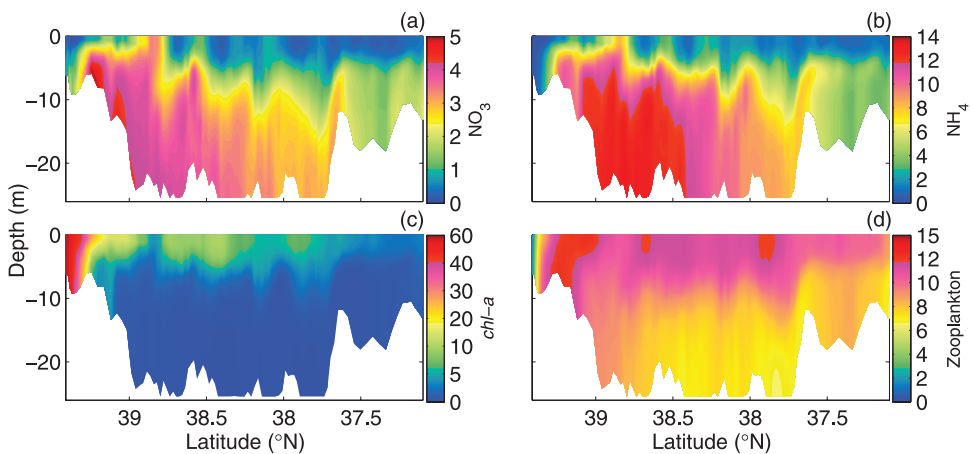

Figure 7. Distributions of (a) NO_3, (b) NH_4, (c) phytoplankton (*chl-a*), (d) zooplankton for an along-channel section at day at day 210 (1 Aug), all in units of m Mol N m^{-3}.
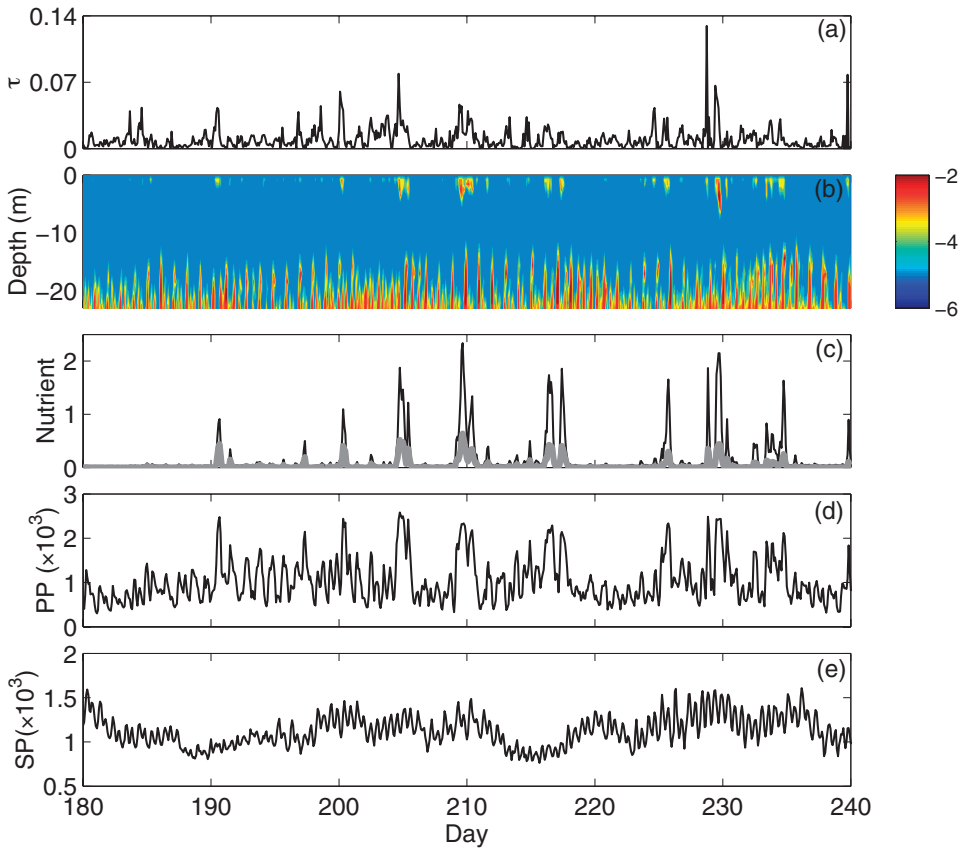
Figure 8. (a) Time series of wind stress magnitude (Nm^{-2}), (b) time evolution of the logarithm of vertical diffusivity (m^2s^{-1}). Time series of (c) surface NO_3 (grey) and NH_4 (black) concentration (m Mol Nm^{-3}), (d) euphotic-layer primary productivity and (e) water-column secondary productivity (mg C $m^{-2}d^{-1}$) at the location of CBOS mid-bay station.

diffusivity and time series of surface NO_3 and NH_4, euphotic-layer PP, and water-column integrated secondary productivity at a mid-Bay location that coincides with a mooring of the Chesapeake Bay Observing System (see Fig. 1c for its location). We also plot the observed time series of wind stress magnitude for comparison (Fig. 8a). Over the two-month period (July and August), a series of weather events occurred with wind stress $> \approx 0.05$ N m^{-2}. The vertical eddy diffusivity k_v inferred from the ROMS model was high in the bottom boundary layer and showed the expected variations at tidal frequencies, i.e., fluctuating at semi-diurnal/diurnal frequencies and modulating over the spring-neap tidal cycle (cf. Li and Zhong, 2009). The diffusivity was weak in the stratified pycnocline. However, k_v increased to large values in the surface layer during those strong wind events (Fig. 8b). Surface NO_3 and NH_4 were depleted at most times. However,

surface NH_4 showed several spikes corresponding to the wind events (Fig. 8c), e.g. on days 200, 205, 209, 228, 229. During days 216 and 217, wind stress was relatively low but k_v increases to large values in the surface layer, leading to surges in surface NH_4. Turbulent mixing in the surface layer depends not only on the instantaneous wind speed but also on current shear in the water column. Strong mixing is generated when the shear is strong enough to overcome stabilizing buoyancy force. The spikes in surface NH_4 in turn led to short-term surges in primary productivity to over twice background rates (Fig. 8d). Since zooplankton have a slower growth rate than phytoplankton, the time series of secondary productivity was less spiky, but also showed broad peaks of enhanced productivity over cumulative wind events (Fig. 8e).

These model results demonstrate that wind-induced strong mixing events can recharge the surface euphotic layer with nutrients and lead to enhanced plankton production. Such short events may contribute significantly to total summer productivity, as documented by limited observational studies. For example, Yeager *et al.* (2005) observed elevated PP in the lower Bay in response to a summer wind event that delivered benthic nutrients to the surface layer. Similarly, a strong fall bloom was observed in Chesapeake Bay after passage of Hurricane Isabel in September 2003 (Miller *et al.,* 2006b).

c. Seasonal cycle

Now we examine the seasonal cycle of plankton biomass and productivity. Figure 9 shows the annual time series of euphotic-layer *chl-a* and PP calculated from the coupled biophysical model. To facilitate comparisons with observations by Harding *et al.* (2002), we apply a unit conversion of 1 m Mol N m^{-3} to 1 mg m^{-3} *chl-a* and C:N of 6.6 to the model outputs. We also divide Chesapeake Bay into lower Bay (polyhaline, regions 1 and 2), mid-Bay (mesohaline, regions 3 and 4) and upper Bay (oligohaline, regions 5 and 6) (see Fig. 1c) since they represent three different salinity regimes to average limited observational data (Adolf *et al.,* 2006). The averaged *chl-a* over the entire Bay reached a maximum in March and remained stable at lower concentrations in summer and fall (Fig. 9a). In contrast, PP showed a broad maximum, corresponding to peaks in PAR and water temperature in summer (Fig. 9b). NO_3 was exhausted in the mid- and lower Bay during summer, and regenerated nutrients NH_4 sustained high PP. Time series of PP exhibited substantial fluctuations at subtidal frequencies, particularly strong during summer months. As discussed in Section 3b, these short-term surges in PP were caused by wind-induced mixing events.

Significant regional differences of *chl-a* and PP existed between the sub-regions of the Bay, as shown in Figure 9. These differences included a pronounced spring bloom in the mid- and lower Bay that was absent in the upper Bay, and a decrease of phytoplankton biomass during summer in both the mid- and lower Bay, contrasted with an annual maximum in the upper Bay. These differences arose because the Bay responded to time-varying nutrient and sediment loading. Whereas the spring freshet supplied nutrients to the upper Bay, high turbidity/low light suppressed phytoplankton production there.
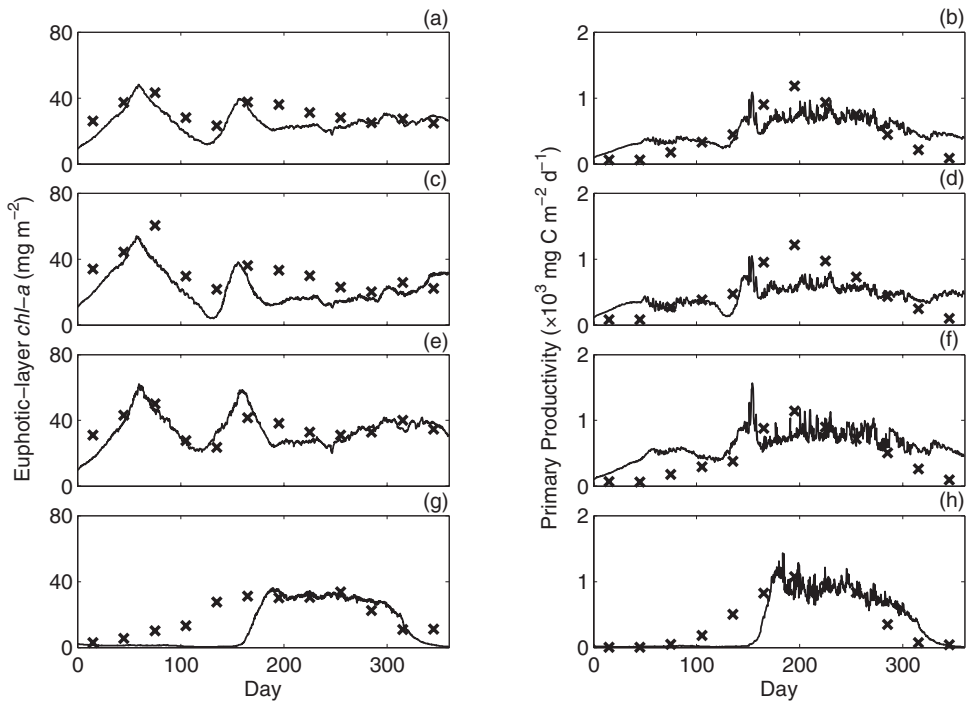
Figure 9. Annual time series of predicted (solid line) and observed (cross) euphotic-layer *chl-a* (left panels) and primary productivity (right panels) averaged over whole Bay (a/b), lower Bay (c/d), mid-Bay (e/f) and upper Bay (g/h).

Consequently, unconsumed nutrients reached the mid- and lower Bay to support plankton production in those downstream regions. The mid- and lower Bay benefited from the nutrient supply while still having sufficient light to support optimal growth. This situation was somewhat reversed during summer when the freshwater flow was much reduced. Improvement in water clarity and proximity to the nutrient source (albeit small) resulted in higher plankton biomass in the upper Bay. In contrast, phytoplankton growth in the mid- and lower Bay was constrained by both nutrient availability and zooplankton grazing so that phytoplankton biomass was lower than during the spring bloom.

d. Skill assessment

Now we compare model results with observational estimates of *chl-a* and PP as well as measurements of nutrient concentrations. Surface *chl-a* concentrations were obtained from ocean-color measurements using radiometers mounted on a light aircraft (e.g. Harding *et al.,* 1994). Flights were conducted 20 to 30 times a year on a set of tracks covering the mainstem of the Bay. The euphotic-layer integrated *chl-a* was computed as the product of the surface *chl-a* and euphotic-layer depth, estimated as the 1% isolume from Secchi depth.

PP was measured in the simulated *in situ* ^{14}C incubations conducted on ship board during field cruises or calculated by applying a regionally validated depth-integrated model (based on Vertically Generalized Productivity Model) to remotely sensed observations, as described in Harding *et al.* (2002). These estimates of euphotic-layer *chl-a* and PP were then spatially averaged to obtain Bay-wide and regional averages for comparison with model predictions.

Time series of euphotic-layer *chl-a* and PP show a general agreement between the model outputs and observations (Fig. 9). Averaged over the whole Bay, *chl-a* reached a maximum during the spring while PP reached its maximum during the summer. Therefore, the coupled biophysical model captures the major observed features of the annual phytoplankton cycle in Chesapeake Bay. Regional differences in the *chl-a* time series are also captured by the model, although the model underestimates the biomass increase in the upper Bay during spring and underpredicts the summer *chl-a* concentration in the lower Bay. The model-predicted time series of PP is in reasonable agreement with the observed annual cycle, but the model underpredicts spring productivity in the upper Bay and summer productivity in the lower Bay.

In addition to *chl-a* and PP, we compare predicted and observed DIN (sum of NO_3 and NH_4) concentrations in the Bay. Nutrient concentrations show a strong gradient in the along-channel direction. Much information would be lost if we aggregate nutrients into the three regions. Instead we compare the surface DIN distribution along the center axis of the Bay. CBP samples a number of monitoring stations along this longitudinal transect at monthly or biweekly intervals. To avoid undersampling in some months and obtain more robust statistics, DIN is averaged over 3 months to produce seasonal means while the vertical bars in Figure 10 indicate the standard derivations from the means. Figure 10 shows the model-data comparisons of the along-channel DIN distribution for the four seasons. The modelled DIN fields follow the observed pattern in space and time reasonably well, although the model underpredicts DIN concentrations in the upper Bay during summer and fall.

We can quantitatively assess the model's skill by using Taylor (Taylor, 2001) and Target diagrams (Jolliff *et al.*, 2009). A brief explanation of these diagrams is given in the Appendix. Figure 11 shows the Taylor and Target diagrams comparing model (Run C) predictions with observations. The correlation coefficient r^2 for all quantities exceeds 0.7, suggesting that the model does a good job in capturing the phase information in the time series of *chl-a* and PP and in the along-channel distributions of DIN. In terms of nutrient predictions, the model reproduces the amplitude of the observed gradient in DIN during winter and spring but underpredicts it during summer and fall (Fig. 11a). This discrepancy is mainly caused by underestimates of NO_3 in the upper Bay by this model (see Figs. 10c and d). Furthermore, the predicted mean DIN concentration is about the same as that observed during winter, but lower during the other three seasons (Fig. 11b). The total rms (root-mean-square) errors for along-channel nutrient distributions were 12.2, 14.3, 6.9 and 13.0 m Mol N m^{-3} during winter, spring, summer and fall seasons, respectively. r^2 was
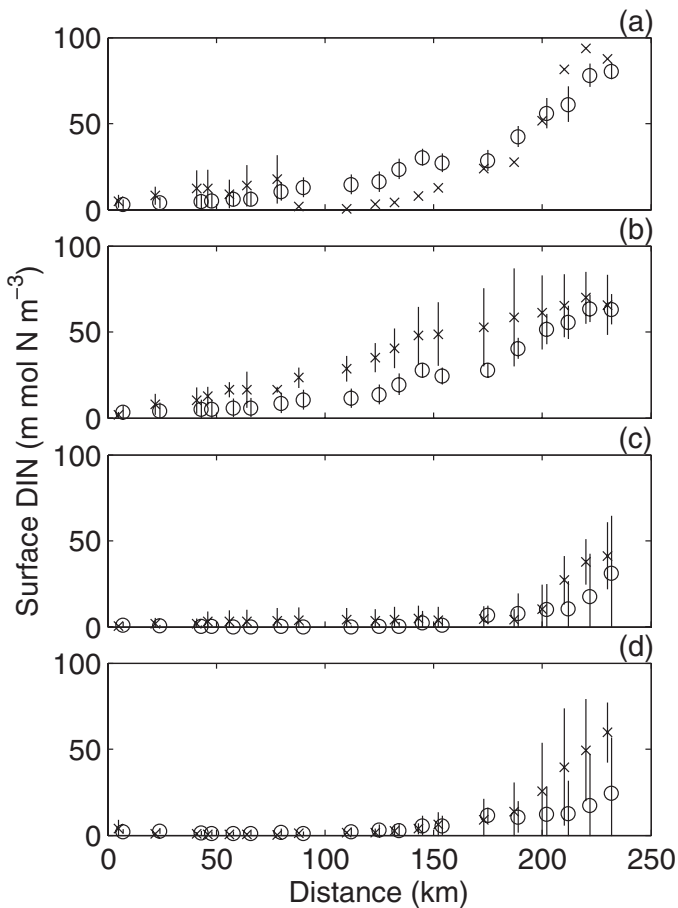
Figure 10. Comparison of predicted (open circle) and observed (cross) nutrient concentration at
   monitoring stations aligned along the center axis of Chesapeake Bay: averages for (a) winter, (b)
   spring, (c) summer and (d) fall seasons. Vertical lines represent standard deviations from the
   seasonal averages.

0.92, 0.94, 0.91 and 0.94, while the skill parameter (see the Appendix for the definition)
reached 0.95, 0.90, 0.88 and 0.72 for the four seasons.

The coupled biophysical model also performs well to predict the centered patterns and
amplitudes of seasonal variations of *chl-a* for the whole Bay and its sub-regions (Fig. 11a).
The correlation coefficient r^2 is around 0.7. The amplitudes agrees within $\pm$ 20%.
However, the annual mean *chl-a* predicted from the model is consistently lower than the
mean derived from ocean-color measurements (Fig. 11b). The total rms errors for *chl-a* are
7.0, 11.9, 6.5 and 11.4 mg m^{-3} for the whole, lower, mid and upper Bay, with the average
relative error at 23% (see Table 3). r^2 between predicted and observed PP exceeds 0.8 in all
regions as the model captures the annual cycle quite effectively. However, the model
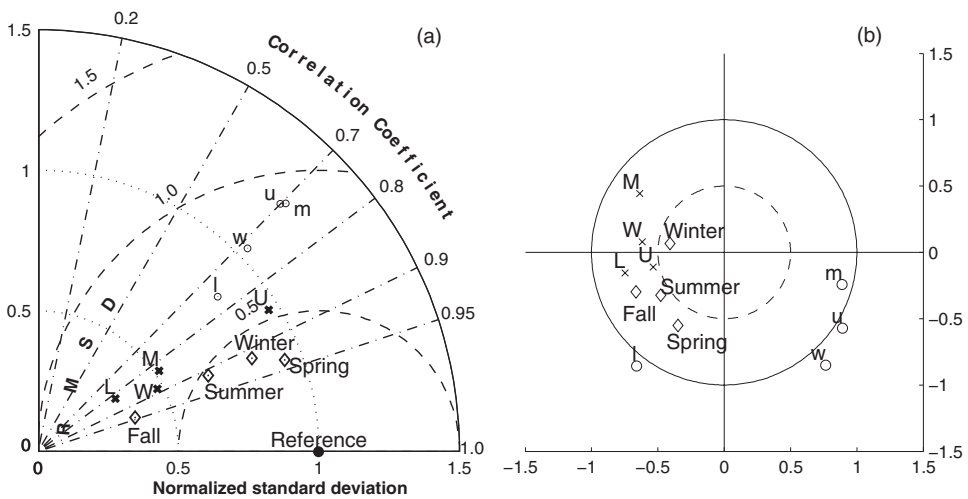
Figure 11. (a) Taylor and (b) Target diagrams for comparing the predicted and observed euphotic-layer *chl-a* (open circles, lower cases) and primary productivity (crosses, upper cases) averaged over whole Bay (W and w), lower Bay (L and l), mid-Bay (M and m) and upper Bay (U and u), and for comparing the predicted and observed nutrient concentration (diamonds) along the center axis of Chesapeake Bay during winter, spring, summer and fall seasons.

significantly underestimates the amplitude of seasonal variation of PP in the lower and mid Bay. PP estimated from the VGPM model shows very low values in the beginning and ending months of 1997, but the ocean-color measurements on which the VGPM model is based were sparse during those times and may have affected the accuracy of its estimates. The predicted PP is higher than the VGPM-based observational estimates during fall, which is a main reason why the predicted PP standard derivation is significantly smaller than the observed. On the other hand, it is encouraging to note that biases in PP are relatively small. Other modelers have also found that PP is more difficult to predict than *chl-a* concentrations (e.g. Lima and Doney, 2004; Fennel *et al.,* 2006).

4. Sensitivity analysis of plankton predictions

Model results presented in Section 3 are based on a single model run (Run C) with a fixed set of biological parameter values. In this section we examine the sensitivity of key plankton metrics to changes in biological rate parameters and physical forcing. We investigate if properties such as AIP are sensitive to changes in biological rate parameters (within observed ranges) and to different formulations of some biogeochemical processes. Consequently we can assess the robustness of predictions from the biogeochemical model. We also use the coupled biophysical model to examine the sensitivity of model results to changes in climatic and meteorological forcing such as river runoff, wind speed, temperature and incoming solar radiation. Although these numerical experiments do not directly

Table 2. Model runs used to examine the sensitivity to variations in biological parameters.

Group Name	Run Name	Description
Group A1	Run C	Linear function Eq. 10 for V_p.
	Run VX	Exponential function Eq. 11 for V_p.
	Run VE	Eppley's curve Eq. 12 for V_p.
Group A2	Run C	$\alpha = 0.065$.
	Run AL	$\alpha = 0.048$.
	Run AS	Seasonally-varying α: 0.065 (1 June to 30 Sep) and 0.048 at other times.
Group A3	Run C	K_{PAR} doubled in regions 5 and 6.
	Run KO	K_{PAR} recovered to interpolated values.
	Run KP	No PO_4 limitation.
Group A4	Run C	Exponential function for remineralization rate: Eq. 13 for t_{Dremin}
	Run RL	Linear function for remineralization rate: Eq. 14 for t_{Dremin}.
Group A5	Run C	Phytoplankton mortality rate $t_{Pmort} = 0.01$.
	Run ML	Phytoplankton mortality rate $t_{Pmort} = 0.1$.

simulate interannual variability in the plankton, they offer a clean test of the model's sensitivity to specific climatic and meteorological forcing. Several different climatic factors may vary simultaneously between consecutive years. It may be difficult to tease out the effects of individual forcing without conducting the sensitivity analyses first.

a. Sensitivity to variations in biological parameters

We conducted sensitivity studies to ascertain how model predictions respond to changes in specific biological parameters within the ranges observed in the Bay. The five-component biogeochemical model has a total of 14 parameters and it is not computationally feasible to explore all combinations of these parameters. Rather, we focus on five aspects of model parameterizations that we expect to strongly influence plankton dynamics: (1) temperature-dependent maximum phytoplankton growth rate V_p; (2) initial slope of the P-I curve α; (3) light attenuation coefficient K_{PAR}; (4) detritus remineralization rate t_{Dremin}; and (5) phytoplankton mortality rate t_{Pmort}. Other parameters are fixed at their respective typical values (as in Run C). These include: (1) half-saturation constants for uptakes of nitrate K_{NO3} and ammonium K_{NH4}, and zooplankton grazing K_p; (2) grazing efficiency AE_N; (3) zooplankton mortality t_{Zmort}, metabolism t_{Zbmet} and excretion Q_{excr} rates; (4) sinking speeds for phytoplankton L_{vp} and detritus L_{vd} (see Table 1 for the parameter values). We conducted a total of 9 model runs and grouped them into 5 separate groups (Table 2).

Two Bay-wide measures of the plankton cycle are used to quantify differences between model runs: annual-mean euphotic-layer *chl-a* (AMC) and annual-integral production (AIP). To evaluate how each model run reproduces the observed plankton annual cycle, we also calculate regression coefficient r^2, rms errors, and skill scores for the annual time series of Bay-averaged *chl-a* and PP (such as those shown in Figs. 9a and 9b). In Run C,

Table 3. Summary of the model sensitivity to biological parameters where AMC and AIP stand for annual mean euphotic-layer *chl-a* and annually-integrated primary productivity averaged over Chesapeake Bay.

Run Name	AMC (mg m^{-2})	r^2	rms (mg m^{-2})	skill	AIP (g Cm^{-2} yr^{-1})	r^2	rms (g Cm^{-2} d^{-1})	Skill
Observations	30.0				170			
Run C	25.4	0.72	7.0	0.72	180	0.89	230	0.82
Run VX	20.7	0.79	10.9	0.59	180	0.86	200	0.89
Run VE	15.2	0.81	16.1	0.46	127	0.83	255	0.80
Run AL	19.1	0.85	12.1	0.54	166	0.92	190	0.89
Run AS	24.2	0.75	7.8	0.69	204	0.87	241	0.82
Run KO	35.5	0.05	10.8	0.45	262	0.82	332	0.77
Run KP	39.1	0.18	12	0.48	280	0.85	361	0.76
Run RL	26.6	0.65	6.6	0.73	225	0.86	258	0.83
Run ML	11.4	0.12	22.2	0.33	145	0.93	155	0.95

AMC is 25.4 mg m^{-2} and AIP is 180 g C m^{-2}yr^{-1}. Observations based on monthly or bi-weekly sampling give AMC of 30 mg m^{-2} and AIP of 170 g C m^{-2}yr^{-1} (see Table 3).

In the first group (A1) of model experiments (Runs C, VX, VE), we examine how different formulations for the temperature dependence of maximum phytoplankton growth rate V_p affect model predictions. Run C uses a linear fit to observed V_p (Eq. 10) for the Bay; Run VX uses an exponential fit to these same data (Eq. 11): and Run VE uses an Eppley function (Eq. 12). Figures 12a and 12b compare the time series of euphotic-layer *chl-a* and PP among the three runs. Spring bloom size is directly related to the value of V_p at spring temperatures (between 5 and 15 degrees) so that it is largest in Run C and smallest in Run VE. Hence AMC is smaller in Runs VX and VE than in Run C because they generate smaller spring blooms (Table 3). Run VX has higher summer productivity than Run C because its V_p values are higher at summer temperatures. Run VE has lower V_p values at all temperatures and thus lower AIP. Overall Runs C and VX produce similar predictions for AMC and AIP because their V_p functions are empirical fits to the *in-situ* data collected in the Bay. In contrast, the Eppley's function developed for the open-ocean applications predicts significantly lower (>30%) AMC and AIP for Chesapeake Bay.

In the second group (A2) of numerical experiments (Runs C, AL, AS), we examine how the slope α of the P-I curve affects model predictions. In Run C, α is set at 0.065, and in Run AL α is 0.048. In Run A3 we allow α to vary seasonally, using 0.065 between June 1 and September 30 and 0.048 at other times (Harding *et al.,* 2002). As shown in Figures 12c and 12d, there are relatively minor differences in the annual time series of *chl-a* and PP among the three runs. The only notable difference is that Run AL has a smaller spring bloom size. AIP varies slightly with the α value. AIP in Run AL is about 8% lower whereas that in Run AS is about 13% larger than Run C. In summary, neither AMC and AIP are very sensitive to values of α within the observed range for Chesapeake Bay.

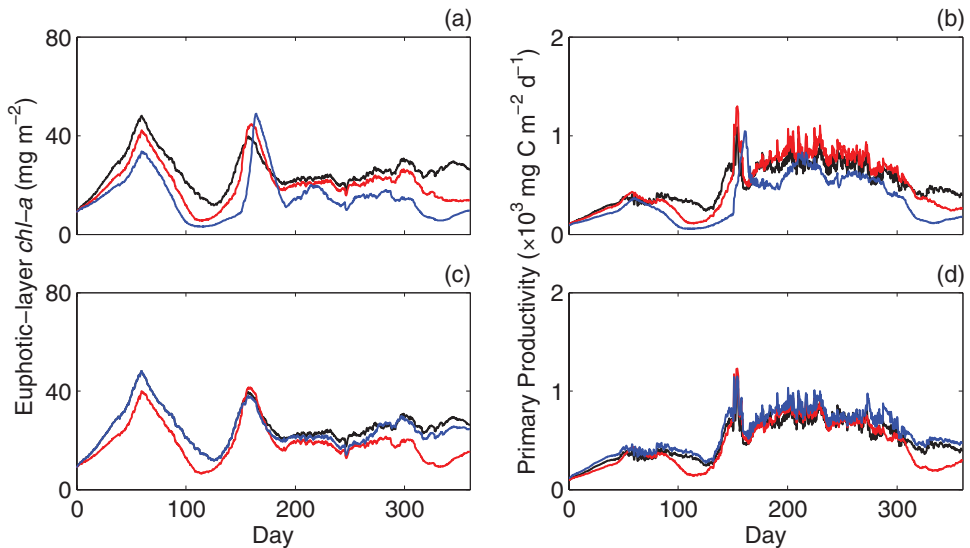In the third group (A3) of numerical experiments, we examine how light attenuation

Figure 12. Comparison of euphotic-layer *chl-a* (left panels) and primary productivity (right panels) averaged over whole Bay for the model runs in Group A1 (upper panels) and Group A2 (lower panels). In Group A1 (a/b), Run C (black), Run VX (red) and Run VE (blue) correspond to linear, exponential and Epply's functions for phytoplankton intrinsic growth rate. In Group A2 (c/d), Run C (black), Run AL (red) and Run AS (blue) correspond to $\alpha = 0.065$, 0.048 and a seasonally varying function.

coefficients and phosphorous limitation in the upper Bay affect model predictions. Few optical measurements are made in the upper Bay with most in the less turbid central shipping channel, as discussed above. When we use those data to form algebraic averages of K_{PAR} for regions 5 and 6, the model overestimates PP in the upper Bay. In Run C we double K_{PAR} values for regions 5 and 6. In Run KO we use observed K_{PAR} without the empirical adjustment. With smaller K_{PAR} values in Run KO, both plankton biomass and PP are significantly higher in the upper Bay (compare red and black lines in Fig. 13). In contrast, changing upper Bay K_{PAR} has much smaller impacts on the mid- and lower Bay. Hence model predictions for the mid and lower Bay are not very sensitive to the results in the upper Bay. Averaged over the whole Bay, AMC in Run KO is 40% higher than in Run C. Although PP in the upper Bay is about twice as high in Run KO as in Run C, AIP for the whole Bay is only 40% higher as the narrow upper Bay represents a relatively small area of the total. These discrepancies demonstrate that accurate determinations of K_{PAR} in the upper Bay are essential to obtain accurate retrievals from the coupled model. Another relevant issue is the suggestion of Fisher *et al.* (1992) that phosphorous rather than nitrogen is the limiting nutrient in low-salinity waters of the Bay. We take the approach developed by Xu and Hood (2006) to consider phosphorous limitation in Run C. To study this effect, we remove phosphorous limitation in Run KP and compare the results with Run C (Fig.
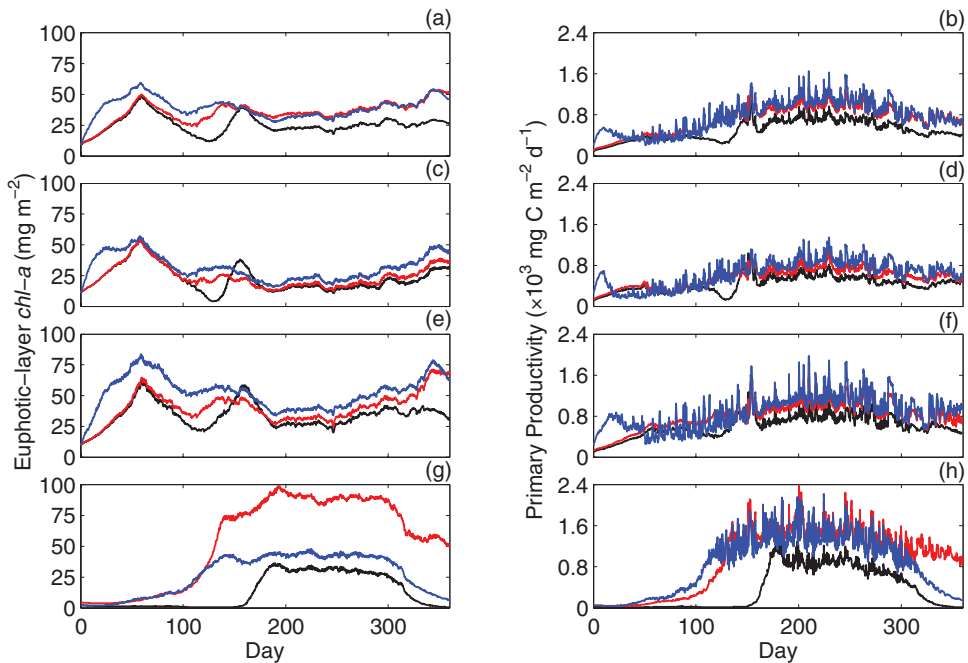
Figure 13. Comparison of euphotic-layer *chl-a* (left panels) and primary productivity (right panels) averaged over whole Bay (a/b), lower Bay (c/d), mid-Bay (e/f) and upper Bay (g/h) for three model runs: Run C (black), Run KO (red) and Run KP (blue), corresponding to different formulations of upper-bay light attenuation and PO$_4$ limitation.

13). This produces a larger spring bloom in the mid Bay but *chl a* in the upper Bay is in better agreement with observations. Removing phosphorous limitation also produces higher PP in the upper Bay (Fig. 13h).

In the fourth group (A4) of numerical experiments (Run C and RL), we test the sensitivity of model predictions to parameterizations of the remineralization rate. In Run C we use an exponential function (Eq. 13), and in Run RL we use a linear function of temperature (Eq. 14). There are minor differences in AMC between the two runs, although AIP in Run RL is 25% larger than in Run C (see Table 3). Essential elements of the remineralization terms are that the remineralization rate is an increasing function of temperature, detritus is converted to NH$_4$, and summer PP is sustained by mixing processes that inject regenerated nutrients into the euphotic layer.

In the fifth group (A5) of numerical experiments (Runs C and ML), we examine how the phytoplankton mortality rate affects model predictions of AMC and AIP. It is difficult to estimate the mortality rate from observations. In Run C we set t_{Pmort} to 0.01. In Run ML t_{Pmort} was 0.1. Both values are in the range of reported observations (e.g. Fennel *et al.,* 2006). AMC in Run M is about half of that in Run C, whereas AIP is 19% lower (see Table 3).

Table 4. Model runs used to examine the sensitivity to changes in physical forcing.

Group Name	Run Name	Description
Group B1	Run C	Observed runoff.
	Run RD	Runoff doubled.
	Run RH	Runoff halved.
Group B2	Run C	Observed wind forcing.
	Run WD	Wind stress doubled.
	Run WN	Wind forcing switched off.
Group B3	Run C	Observed air temperature.
	Run TI	Temperature increased by 2°C.
	Run TD	Temperature decreased by 2°C.
Group B4	Run C	Observed surface PAR.
	Run PI	Surface PAR increased by 30%.
	Run PD	Surface PAR decreased by 30%.

The higher mortality rate we use in Run ML significantly reduces the magnitudes of the spring bloom and the summer PP.

In summary, nine model runs were conducted to explore the effects of alternative parameter values and different formulations of some biogeochemical processes. Although this set of runs is far from exhaustive in the 14-dimensional parameter space of the coupled model, we selected model elements expected to exert more important controls than other parameters that were fixed. It is satisfying to find a general consistency between the different model runs, as shown in Table 3. Both AMC and AIP range within 50%, suggesting a degree of robustness of the model results.

b. Sensitivity to changes in physical forcing

River runoff, wind forcing, temperature and light field are four types of climatic and meteorological forcing that are expected to exert important controls on phytoplankton growth, but their precise effects are not well studied in Chesapeake Bay. We conducted four groups of numerical experiments to examine how plankton biomass and productivity vary in response to changes in these physical forcing fields (see Table 4).

In the first group (B1) of model experiments (Runs C, RD, RH), we examine how the magnitude of river runoff affects euphotic-layer *chl-a* and PP averaged over the whole Bay and its subregions. Analysis of the long-term record of river flow over the past century reveals that the annual mean discharge varies between 1000 and 3500 m^3s^{-1}. The mean river discharge for 1997 was about 1600 m^3s^{-1}, slightly below the long-term mean. Run C uses observed river flow rate, Run RD doubles flow rate, and Run RH has half of the observed flow. As shown in Figs. 14a and 14b, both *chl-a* and PP show a strong response to the doubling of the freshwater flow and associated increase of nutrient loading. Increased biomass is particularly pronounced in the mid- and lower Bay regions as higher river flow carries nutrient-rich water further down the estuary. PP is significantly elevated in all

regions of the Bay. AMC is 43.0 mg m^{-2} in Run RD versus 25.4 mg m^{-2} in Run C. AIP is 305 g C m^{-2} yr^{-1} in Run RD versus 180 g C m^{-2} yr^{-1} in Run C (Table 5). Both AMC and AIP increase by about 70% for a doubling of river runoff. In contrast, the response to a 50% reduction of river runoff is less dramatic. AMC is 17.6 mg m^{-2} and AIP is 157 g C m^{-2} yr^{-1} in Run RH, only 30% and 13% smaller than their counterparts in Run C, respectively. These model comparisons suggest nonlinear responses of plankton biomass and productivity to variability of river runoff and nutrient loading.

Our analysis in Section 3 shows that summer winds cause temporary increases of PP. To investigate if these contribute to a net increase in AIP, we conduct second group (B2) of numerical experiments (Runs C, WD, WN). We analysed the time series of wind speeds measured at three weather stations: BWI (Baltimore-Washington International Airport), PRNS (Patuxent River Naval Station) and NIA (Norfolk International Airport) over a five year period between 1994 and 1998. We found that the maximum of the annually averaged wind speed exceeds that of 1997 by about 33%. This translates to 80% increase in the wind stress. Hence the wind stress is doubled in Run WD. In order to further clarify the wind effects, we conduct another run (Run WN) in which the wind forcing is switched off. Figures 14c and 14d compare the time series among the three runs. PP in Run WD is higher with much more pronounced spikes. AIP is 231 g C m^{-2} yr^{-1} in Run WD versus 180 g C m^{-2} yr^{-1} in Run C (see Table 5). In contrast, no spikes are found in the PP time series for Run WN in which wind forcing is switched off. It is interesting to note that AMC in Run WN is 38% smaller than Run C but AIP is about the same between Runs C and WN. Wind-induced mixing affects phytoplankton growth in two different ways. On the one hand, winds can inject nutrients to the euphotic layer and enhance PP. One the other hand, they could increase the mixed layer depth such that phytoplankton may be driven to deeper water with lower light exposure, thus reducing PP. The net effect of wind mixing on PP thus depends on the competition between these two factors. In addition to the local winds blowing over the Bay's surface, offshore winds blowing over the adjacent shelf may produce coastal upwelling and import nutrients into Chesapeake Bay, but this nutrient source is expected to be small (see Boynton *et al.,* 1995).

In the third group (B3) of model experiments (Runs C, TI, TD), we examine how temperature change might affect the plankton system in the Bay. Historical records show that global temperature has increased by 1°C since 1880. Global climate models are predicting that temperature in the mid-Atlantic region may increase 1–4°C by the end of 21st century (Najjar *et al.,* 2009). To understand how global warming might affect plankton production in the Bay, we conduct two additional runs: Run TI in which temperature is increased by 2°C and Run TD in which temperature is decreased by the same amount. Table 5 summarizes the results from these runs. AMC increases from 25.4 to 30 mg m^{-2} for 2°C warming but remains about the same for 2°C cooling. AIP increases from 180 to 246 g C m^{-2} yr^{-1} due to warming, but AIP in cooler condition simulated by Run TD is surprisingly higher than Run C.
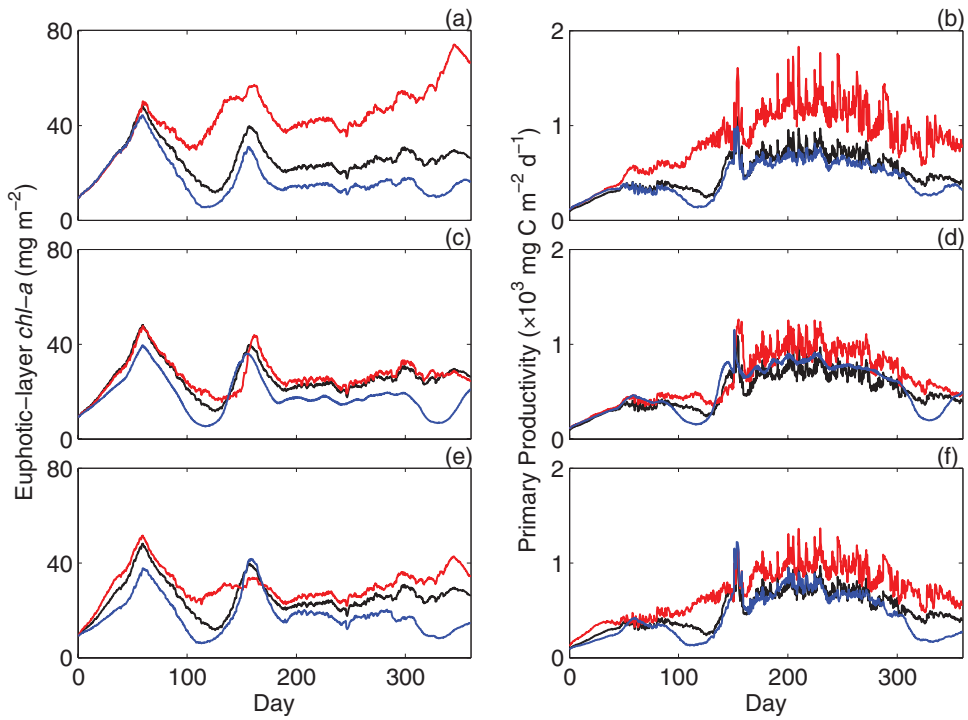
Figure 14. Comparison of euphotic-layer *chl-a* (left panels) and primary productivity (right panels) averaged over whole Bay for the model runs in Groups B1 (upper panels), B2 (middle panels) and B4 (lower panels). Group B1 (a/b) consists of Run C (black), higher-runoff run (RD, red) and lower-runoff run (RH, blue). Group B2 (c/d) consists of Run C (black), double-stress run (WD, red) and no wind forcing run (WN, blue). Group B4 (e/f) consists of Run C (black), higher-PAR run (PI, red) and lower-PAR run (PD, blue).

In the fourth group (B4) of model experiments (Runs C, PI, PD), we examine how the magnitude of surface PAR affects *chl-a* and PP. In Run C, we use daily averaged PAR for 1997. However, Fisher *et al.* (2003) examined the annual cycle of PAR over the past couple of decades and found that PAR can vary about ± 30% over the long-term average, depending the cloud cover and weather conditions in a particular year. To examine the sensitivity of plankton biomass and productivity to PAR, we conduct two more runs: Run PI in which PAR is increased by 30% and Run PD in which PAR is decreased by 30%. Spring bloom size in the mid and lower Bay and summer plankton biomass in the upper Bay are proportional to the PAR values (Fig. 14e). PP also varies with PAR (Fig. 14f). In summary, AMC increases/decreases by 18%/28% and AIP increases/decreases by 38%/22% for the 30% increase/decrease in surface PAR (Table 5).

To summarize, we have examined how the plankton system responds to variations in river runoff, wind forcing, temperature and light level. While the river runoff and associated nutrient loading are the dominant factor affecting *chl-a* and PP, wind-induced

Table 5. Summary of the model sensitivity to variations in physical forcing where AMC and AIP stand for annual mean euphotic-layer *chl-a* and annually-integrated primary productivity averaged over Chesapeake Bay.

Run Name	AMC (mg m^{-2})	AIP (g Cm^{-2} yr^{-1})
Observations	30.0	170
Run C	25.4	180
Run RD	43.0	305
Run RH	17.6	157
Run WD	26.5	231
Run WN	18.3	188
Run TI	30.0	246
Run TD	25.4	216
Run PI	30.0	249
Run PD	18.1	158

mixing significantly enhances summer PP. AMC and AIP increase by about 70% for a doubling of river runoff, but only reduce by 30% and 13% for 50% reduction of river runoff. Doubling of wind stress results in 28% increases in AIP while AMC increases from 25.4 to 30 mg m^{-2} and AIP increases from 180 to 246 g C m^{-2} yr^{-1} for 2-degree warming.

5. Conclusions

We have used a 3D coupled hydrodynamic-biogeochemical model to simulate the annual cycle and regional distributions of plankton biomass and productivity in Chesapeake Bay. The model captures the observed phase lag between the spring *chl-a* maximum and summer PP peak, and shows reasonable skill in reproducing the observed *chl-a,* PP and nutrient distributions. Sensitivity analysis of model simulations for different biological-parameter values and alternative formulations of biogeochemical processes suggest that model predictions are relatively robust. Hence this coupled biophysical model provides a useful tool to explore how physical processes and climate variability affect plankton dynamics in Chesapeake Bay.

Previous research suggested that dead plankton sink and are remineralized to yield regenerated nutrients that support high PP in summer. However, the mechanism for reintroduction of regenerated nutrients into the euphotic layer under strongly stratified conditions that persist in summer had not been satisfactorily explained. Our model demonstrates that episodic wind events in summer inject regenerated nutrients into the surface euphotic layer, leading to short periods of enhanced PP. Since both EPA CBP sampling cruises and aircraft remote-sensing flights are carried out at roughly biweekly or monthly intervals, there have been little observational documentation of the effects of wind mixing on plankton dynamic in Chesapeake Bay. In the future, it would be desirable to schedule remote-sensing flights to capture plankton response to wind events.

The plankton system in Chesapeake Bay shows different responses to variations in river

runoff, wind forcing, temperature and light. While river runoff and associated nutrient loading is the dominant factor affecting *chl-a* and PP, wind-induced mixing may significantly enhance summer PP. Warming promotes phytoplankton growth, but light level affects spring bloom size in the mid- and lower Bay and the summer biomass peak in the upper Bay. These sensitivity analyses based on variable physical forcing lay the groundwork for simulating the interannual variability of the spring bloom and summer PP maximum that have been traced to regional climatic variability (Miller and Harding, 2007). A model capable of capturing past interannual variability may be also used to project the impacts of future climate change on the plankton system in Chesapeake Bay.

APPENDIX

In the Taylor diagram, the correlation coefficient r^2, the centered root-mean-square (rms) error E, and the ratio σ_n of the standard deviations of the model-predicted field (i.e., the test field) and the observed field (i.e., the reference field) are displayed by the location of one point (representing the model field) in relation to the reference point (representing the observed field). The correlation coefficient measures the centered pattern agreement of the variations of the two fields regardless of amplitude; in other words, correlation is high if the test field is correctly phased. The centered rms error measures the difference between the fields with the overall bias removed. The ratio of the standard deviations indicates if the test field overestimates ($\sigma_n > 1$) or underestimates ($\sigma_n < 1$) the amplitude of variations. The reference point is located on the x axis at $\sigma_n = 1$. The radial distance of the test point from the origin indicates the normalized standard deviation ($\sigma_n = \sigma_{mod}/\sigma_{obs}$), its azimuthal position indicates the correlation coefficient, and its distance from the reference point indicates the centered rms error.

The Target diagram provides summary information about the pattern statistics as well as the bias, thus allowing for an assessment of their respective contributions to the total rms. In a simple Cartesian coordinate system, the unbiased rms serves as the X-axis and the bias serves as the Y-axis. By definition, the X-axis (unbiased rms) must always be positive. However, the X<0 region of the Cartesian coordinate space may be utilized if the unbiased rms difference is multiplied by the sign of the standard deviation difference $\sigma_d = $ sign ($\sigma_{mod} - \sigma_{obs}$) (see Jolliff *et al.,* 2009). Again we normalize the quantities by the reference field standard deviation.

In addition to the Taylor and Target diagrams, we apply a model "skill parameter" used by Warner *et al.* (2005b) in their simulations of the Hudson River estuary:

$$Skill = 1 - \frac{\sum_{i=1}^{N} |\eta_{mod} - \eta_{obs}|^2}{\sum_{i=1}^{N} (|\eta_{mod} - \bar{\eta}_{obs}| + |\eta_{obs} - \bar{\eta}_{obs}|)^2} \tag{A1}$$

where η is the variable being compared, $\bar{\eta}$ its time mean, and the subscripts mod and obs refer to model outputs and observations, respectively. Perfect agreement between model outputs and observations yields a skill of 1.0 whereas complete disagreement yields a skill of 0.

REFERENCES

Adolf, J. E., C. L. Jordan, W. D. Miller, M. E. Mallonee and L. W. Harding, Jr. 2006. Phytoplankton floral composition, biomass, and primary productivity in Chesapeake Bay. Estuar. Coast. Shelf Sci., *67*, 108–122.

Arhonditsis, G. B. and M. T. Brett. 2004. Evaluation of the current state of mechanistic aquatic biogeochemical modeling. Mar. Ecol. Prog. Ser., *271,* 13–26.

Boicourt, W. C. 1992. Influences of circulation processes on dissolved oxygen in the Chesapeake Bay, *in* Oxygen Dynamics in Chesapeake Bay: A Synthesis of Research, D. Smith, M. Leffler, and G. Mackiernan, eds., University of Maryland Sea Grant College, College Park, MD, 7–59.

Boynton, W. R., J. H. Garber, R. Summers and W. M. Kemp. 1995. Inputs, transformations, and transport of nitrogen and phosphorus in Chesapeake Bay and selected tributaries. Estuaries, *18,* 285–314.

Carter, H. H. and D. W. Pritchard. 1988. Oceanography of Chesapeake Bay, *in* Hydrodynamics of Estuaries: Dynamics of Partially-Mixed Estuaries, B. Kjerfe, ed., Vol. 1. CRC Press, 1–16.

Cerco, C. 1995. Simulation of long-term trends in Chesapeake Bay Eutrophication. J. Environ. Eng. ASCE., *121,* 298–310.

Cerco, C and T. Cole. 1993. Three-dimensional eutrophication model of Chesapeake Bay. J. Hydro. Eng., *119,* 1006–1025.

Chen, C., R. C. Beardsley and P. J. S. Franks. 2001. A 3-D prognostic numerical model study of the Georges Bank ecosystem. Part I: Physical model. Deep-Sea Res. II, *48,* 419–456.

Eppley, R. W. 1972. Temperature and phytoplankton growth in the sea. Fishery Bull., *70,* 1063–1085.

Evans, G. T. and J. S. Parslow. 1985. A model of annual plankton cycles. Bio. Oceanogr., *3,* 327–347.

Fasham, M. J. R., H. W. Ducklow and S. M. McKelvie. 1990. A nitrogen-based model of plankton dynamics in the ocean mixed layer. J. Mar. Res., *48,* 591–639.

Fennel, K. 1999. Interannual and regional variability of biological variables in a coupled 3-D model of the western Baltic. Hydrobiologia, *393,* 25–33.

Fennel, K., J. Wilkin, J. Levin, J. Moisan, J. O'Reilly and D. Haidvogel. 2006. Nitrogen cycling in the Middle Atlantic Bight and implications for the North Atlantic nitrogen budget: Results from a three-dimensional model. Global Biogeochem. Cycles, *20,* GB3007, doi:10.1029/2005GB002456.

Fisher, T. R., A. B. Gustafson, G. M. Radcliffe, K. L. Sundberg and J. C. Stevenson. 2003. A long-term record of photosynthetically available radiation (PAR) and total solar energy at 38.6° N, 78.2° W. Estuaries, *26,* 1450–1460.

Fisher, T. R., A. B. Gustafson, K. Sellner, R. Lacouture, L. W. Haas, R. L. Wetzel, R Magnien, D.

Everitt, B. Michaels and R. Karrh. 1999. Spatial and temporal variation of resource limitation in Chesapeake Bay. Mar. Biol., *133,* 763–778.

Fisher, T. R., E. R. Peele, J. W. Ammerman and L. W. Harding, Jr. 1992. Nutrient limitation of phytoplankton in Chesapeake Bay. Mar. Ecol. Prog. Ser., *82,* 51–63.

Franks, P. J. S. and C. Chen. 2001. A 3-D prognostic model study of the ecosystem over Georges Bank and adjacent coastal regions. Part II: Coupled biological and physical model. Deep-Sea Res., *48,* 457–482.

Harding, L. W., Jr., E. C. Itsweireand W. E. Esaias. 1994. Estimates of phytoplankton chlorophyll biomass in the Chesapeake Bay from aircraft remote sensing of chlorophyll concentrations, 1989–1992. Remote Sens. Environ.,*49,* 41–56.

Harding, L. W., M. E. Mallonee and E. S. Perry. 2002. Toward a predictive understanding of primary productivity in a temperate, partially stratified estuary. Estuar. Coast. Shelf Sci.,*55,* 437–463.

Harding, L. W., Jr., and E. S. Perry. 1997. Long-term increase of phytoplankton biomass in Chesapeake Bay. Mar. Ecol. Prog. Ser., *157,* 39–52.

Hilton, T. W., R. G. Najjar, L. Zhong and M. Li. 2008. Is there a signal of sea-level rise in Chesapeake Bay salinity? J. Geophys. Res., *113,* C09002, doi:10.1029/2007JC004247.

Johnson, B. H., K. W. Kim, R. E. Heath, N. N. Hseish and H. L. Butler. 1993. Verification of a three-dimensional hydrodynamic model of Chesapeake Bay. J. Hydra. Eng., ASCE, *119,* 2–20.

Johnson, M. D., M. Rome and D. K. Stoecker. 2003. Microzooplankton grazing on *Prorocentrum minimum* and *Karlodinium micrum* in Chesapeake Bay. Limnol. Oceanogr., *48,* 238–248.

Jolliff, J. K., J. C. Kindle, I. Shulman, B. Penta, M. A. M. Friedrichs, R. Helber and R. A. Arnone. 2009. Summary diagrams for coupled hydrodynamic-ecosystem model skill assessment. J. Mar. Syst., *76,* 64–82.

Kana, T. M., M. B. Sullivan, J. C. Cornwell and K. M. Groszkowski. 1998. Denitrification in estuarine sediments determined by membrane inlet mass spectrometry. Limnol. Oceanogr., *43,* 334–339.

Kemp, W. M. and W. R. Boynton. 1992. Benthic-pelagic interactions: nutrient and oxygen dynamics, *in* Oxygen dynamics in the Chesapeake Bay, D. E. Smith, M. Leffler and G. Mackiernan, eds., Maryland Sea Grant College, 149–221.

Kemp, W. M., P. A. Sampou, J. M. Caffrey, M. Mayer, K. Henriksen and W. R. Boynton. 1990. Ammonium recycling versus denitrification in Chesapeake Bay sediments. Limnol. Oceanogr., *35,* 1545–1563.

Li. M. and L. Zhong. 2009. Flood-ebb and spring-neap variations of mixing, stratification and circulation in Chesapeake Bay. Cont. Shelf Res., *29,* 4–14.

Li, M., L. Zhong and W. C. Boicourt. 2005. Simulations of Chesapeake Bay estuary: Sensitivity to turbulence mixing parameterizations and comparison with observations. J. Geophys. Res., *110,* C12004, doi:10.1029/2004JC002585.

Li, M., L. Zhong, W. C. Boicourt, S. Zhang and D.-L. Zhang. 2006. Hurricane-induced storm surges, currents and destratification in a semi-enclosed bay. Geophys. Res. Lett., *33,* L02604, doi:10.1029/ 2005GL024992.

—— 2007. Hurricane-induced destratification and restratification in a partially-mixed estuary. J. Mar. Res., *65,* 169–192.

Lima, I. D. and S. C. Doney. 2004. A three-dimensional, multinutrient, and size-structured ecosystem model for the North Atlantic. Global Biogeochem. Cycles, *18,* GB3019, doi:10.1029/ 2003GB002146.

Lomas, M. W., P. M. Glibert, F-K. Shiah and E. M. Smith. 2002. Microbial processes and temperature in Chesapeake Bay: current relationships and potential impacts of regional warming. Global Change Biol., *8,* 51–70.

Malone, T. C. 1992. Effects of water column processes on dissolved oxygen: nutrients, phytoplank-

ton and zooplankton, *in* Oxygen Dynamics in Chesapeake Bay: A Synthesis of Research, D. Smith, M. Leffler and G. Mackiernan, eds., University of Maryland Sea Grant College, College Park, MD, 61–112.

Malone, T. C., L. Crocjer, S. Pike and B. Wendler. 1988. Influence of river flow on the dynamics of phytoplankton production in a partial stratified estuary. Mar. Ecol. Prog. Ser., *48,* 235–249.

Malone, T. C., D. J. Conley, T. R. Fisher, P. M. Glibert and L. W. Harding. 1996. Scales of nutrient-limited phytoplankton productivity in Chesapeake Bay. Estuaries, *19,* 371–385.

Miller, W. D. and L. W. Harding, Jr. 2007. Climate forcing of the spring bloom in Chesapeake Bay. Mar. Ecol. Prog. Ser., *331,* 11–22.

Miller, W. D. and L. W. Harding, Jr. and J. E. Adolf. 2006a. The effects of Hurricane Isabel on Chesapeake Bay phytoplankton dynamics. Geophys. Res. Lett., *33,* L06612, doi: 10.1029/2005GL025658, 2006.

Miller, W. D., L. W. Harding, Jr., D. G. Kimmel, and M. E. Mallonee. 2010. Climate forcing of primary productivity in Chesapeake Bay. Estuar. Coast. Shelf Sci. (submitted).

Miller, W. D., D. G. Kimmel, and L. W. Harding, Jr. 2006b. Predicting spring discharge of the Susquehanna River from a winter synoptic climatology for the Eastern United States. Water Resour. Res., *42,* W05414, doi:10.1029/2005WR004270.

Moisan, J. R., E. E. Hofmann and D. B. Haidvogel. 1996. Modeling nutrients and plankton processes in the California coastal transition zone 2. A three-dimensional physical-bio-optical model. J. Geophys. Res., *101,* C10, 22,677–22,691.

Najjar, R. G., L. Patterson and S. Graham. 2009. Climate simulations of major estuarine watersheds in the Mid-Atlantic region of the United States. Climatic Change, *95,* 139–168.

North, E. W., Z. Schlag, R. R. Hood, M. Li, L. Zhong, T. Gross and V. S. Kennedy. 2008. Larval vertical swimming behavior may influence the dispersal of oysters in Chesapeake Bay. Mar. Ecol. Prog. Ser., *359,* 99–115.

Paerl, H. W., L. M. Valdes, J. E. Adolf, B. M. Peierls and L. W. Harding Jr. 2006. Anthropogenic and climatic influences on the eutrophication of large estuarine ecosystems. Limnol. Oceanogr., *51,* 448–462.

Shchepetkin, A. F. and J. C. McWilliams. 2005. The regional oceanic modeling system: A split-explicit, free-surface, topography-following-coordinate ocean model. Ocean Model., *9,* 347–404.

Song, Y. T. and D. B. Haidvogel. 1994. A semi-implicit ocean circulation model using a generalized topography-following coordinate. J. Comput. Phys., *115,* 228–244.

Steele, J. H. and E. W. Henderson. 1992. The role of predation in plankton models. J. Plankton Res., *14,* 157–172.

Taylor, K. E. 2001. Summarizing multiple aspects of model performance in a single diagram. J. Geophys. Res., *106,* 7183–7192.

Wang, D. P. 1979a. Subtidal sea level variations in the Chesapeake Bay and relations to atmospheric forcing. J. Phys. Oceanogr., *9,* 413–421.

—— 1979b. Wind-driven circulation in the Chesapeake Bay, Winter, 1975. J. Phys. Oceanogr., *9,* 564–572.

Warner, J. C., W. R. Geyer and J. A. Lerczak. 2005a. Numerical modeling of an estuary: A comprehensive skill assessment. J. Geophys. Res., *110,* C05001, doi:10.1029/2004JC002691.

Warner, J. C., C. R. Sherwood, H. G. Arango, B. Butman and R. P. Signell. 2005b. Performance of four turbulence closure models implemented using a generic length scale method. Ocean Model., *8,* 81–113.

White, J. R. and M. R. Roman. 1992. Seasonal study of grazing by metazoan zooplankton in the mesohaline Chesapeake Bay. Mar. Ecol. Prog. Ser., *86,* 251–261.

Xu, J. and R. R. Hood. 2006. Modeling biogeochemical cycles in Chesapeake Bay with a coupled physical-biological model. Estuar. Coast. Shelf Sci., *69,* 19–46.

Yeager, C. L. J., L. W. Harding Jr. and M. E. Mallonee. 2005. Phytoplankton production, biomass and community structure following a summer nutrient pulse in Chesapeake Bay. Aquatic Ecol., *39,* 135–149.

Zhong, L. and M. Li. 2006. Tidal energy fluxes and dissipation in the Chesapeake Bay. Cont. Shelf Res., *26,* 752–770.

Zhong, L., M. Li and M. G. G. Foreman. 2008. Resonance and sea level variability in Chesapeake Bay. Cont. Shelf Res., *28,* 2565–2573.